University of Texas at Arlington

MavMatrix

Mechanical and Aerospace Engineering Theses

Mechanical and Aerospace Engineering Department

2024

EXPERIMENTAL STUDY ON THERMAL PERFORMANCE OF METAL FOAM HEAT SINKS IN SINGLE PHASE LIQUID IMMERSION COOLING

Manish Kumawat

Follow this and additional works at: https://mavmatrix.uta.edu/mechaerospace_theses

Part of the Aerospace Engineering Commons, and the Mechanical Engineering Commons

Recommended Citation

Kumawat, Manish, "EXPERIMENTAL STUDY ON THERMAL PERFORMANCE OF METAL FOAM HEAT SINKS IN SINGLE PHASE LIQUID IMMERSION COOLING" (2024). *Mechanical and Aerospace Engineering Theses*. 1019.
https://mavmatrix.uta.edu/mechaerospace_theses/1019

This Thesis is brought to you for free and open access by the Mechanical and Aerospace Engineering Department at MavMatrix. It has been accepted for inclusion in Mechanical and Aerospace Engineering Theses by an authorized administrator of MavMatrix. For more information, please contact leah.mccurdy@uta.edu, erica.rousseau@uta.edu, vanessa.garrett@uta.edu.

EXPERIMENTAL STUDY ON THERMAL PERFORMANCE OF METAL FOAM HEAT SINKS IN SINGLE PHASE LIQUID IMMERSION COOLING

by

MANISH KUMAWAT

Presented to the Faculty of the Graduate School of
The University of Texas Arlington in Partial Fulfillment
of the Requirements
for the Degree of

MASTER OF SCIENCE IN AEROSPACE ENGINEERING

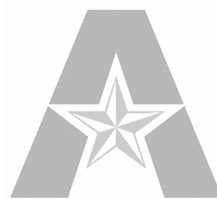

THE UNIVERSITY OF TEXAS AT ARLINGTON

DECEMBER 2023

Copyright © by Manish Kumawat, 2023

All Rights Reserved

ACKNOWLEDGEMENT

It brings me pride to look back and see the faces and hearts of those who have helped me along the way as I stand at the end of this educational journey. This thesis is the result of many people's support and belief, in addition to my own efforts.

First and foremost, I would want to express my sincere gratitude to Dr. Dereje Agonafer, my thesis supervisor, whose knowledge and compassion accord me for providing priceless resources and opportunity to improve my knowledge and skills to serve my achievements in the field of Thermal management and reliability of electronic packaging. Their tolerance and rigorous academic standards have had a lasting impression on my writing, personality, and success.

I would also like to extend my gratitude to the committee members Dr. Abdolhussain Haji Shaikh and Dr. Pratik Vithoba Bansode for providing their time and to the faculty and staff of the Mechanical and Aerospace Engineering department for their continuous support for helping me to deliver valuable inputs. For my research, the atmosphere has served as a workshop and rich environment.

To my research partners and my PhD mentors Gautam Gupta, and Dr. Vivek Cheruvateth Nair, who walked this marathon with me: our conversations, guidance, and weekly questionnaire sessions strengthen my concepts and practical experience. The connection will always be the threads of friendship that I will treasure.

I am indebted to my family for my warmth and affection. Being the quiet, unwavering pillar of support behind my ambitions, sharing in my successes and offering consolation in my defeats all without ever asking for attention.

With gratitude,
Manish Kumawat

DECEMBER 2023

DEDICATION

My Master Thesis Dissertation is Dedicated

to

My Parents

Mrs. Narbada Kumawat

Supervising Professor: **Dr. Dereje Agonafer**

And to My Mentor

Dr. Pratik Bansode

For their Motivation and Kind Support.

TABLE OF CONTENTS

ABSTRACT……………………………………………………………………………….… viii

LIST OF FIGURES……………………………………………………………………..... x

LIST OF TABLES……………………………………………………………..……… xii

LIST OF GRAPHS………………………………………………………...………… xiii

Chapter 1 1

1.1. Introduction 1

1.2. Power Consumption.. 2

Chapter 2 4

2.1. Types of Cooling Techniques 4

2.1.1. Direct contact liquid cooling 4

2.1.1.1. Air Cooling: 4

2.1.1.2. Spray Cooling: 5

2.1.1.3. Jet impingement cooling:... 7

2.1.1.4. Immersion Cooling: 9

2.1.1.5. Droplet Electrowetting:.. 10

2.1.2. Indirect contact cooling 11

2.1.2.1. Microchannel Cooling: 11

2.1.2.2. Heat Pipe Cooling:.. 12

2.1.2.3. Thermoelectric cooling:... 14

2.1.2.4. Vapor Chamber:.. 14

2.1.2.5. PCM Based Cooling: 15

Chapter 3 17

3.1. Coolant Fluids 17

3.2. Coolants used in immersion cooling. 18

3.3. Dielectric synthetic Fluid (EC-100) 18

Chapter 4 20

4.1. Metal Foam 20

4.1.1. Open-Cell Metal Foams 20

4.1.2. Closed-Cell Metal Foams 20

4.1.3. Applications: 21

4.2. Making of Metal Foams: 22

4.2.1. Foaming by Gas Injection 23

4.2.2. Foaming with Blowing Agents 24

4.2.3. Solid–gas Eutectic Solidification (Gasars). 25

4.2.4. Casting Methods 25

4.2.5. Powder Compact Melting Technique 26

4.3. Characterization 27

Chapter 5 30

5.1 Boundary Conditions: 30

5.2 Data reduction: 30

5.3 Uncertainty Analysis: 31

Chapter 6 33

Experiment Setup: 33

Methodology: 35

Procedure: 38

Sensor Calibration: 38

Chapter 7 40

Result and Discussions 40

Chapter 8 50

Conclusions 50

Biographical Statement 51

References: 52

ABSTRACT

EXPERIMENTAL STUDY ON THERMAL PERFORMANCE OF METAL FOAM HEAT SINKS IN SINGLE PHASE LIQUID IMMERSION COOLING

Manish Kumawat, MS

The University of Texas at Arlington, 2023

Supervising Professor: **Dr. Dereje Agonafer**

In 1965, Intel co-founder Gordon Moore made the observation that the transistor counts on a chip double with a frequency of approximately every two years. This development resulted in more compact and potent ICs. However, the amount of heat produced on a chip increased proportionally with the number of transistors. Later, in the early 2000s, Dennard Scaling broke down. Transistors became so small that leakage currents (unwanted currents that flow within the transistor) emerged as a significant issue, and they contributed substantially to power consumption and heat generation. These tightly packed transistors produced heat, which decreased their performance and shortening their lifespan as well as causing the IC to fail. As a result, efficient cooling systems became increasingly crucial in electronics, particularly in high-performance computing, to dissipate this heat and maintain the reliability and performance of the devices. Advanced cooling techniques, such as liquid cooling, phase-change cooling, and advanced materials for heat dissipation, are widely used.

Single phase liquid immersion cooling is a method of cooling electronic components where the components are completely immersed in a dielectric liquid (electrically non-conductive). In conditions where high-performance computing and data center applications require significant heat dissipation, single-phase liquid immersion cooling is a more efficient technique than air cooling, particularly in high heat flux, efficient heat removal, uniform cooling, improved

reliability, and longevity of components. The process is termed "single-phase" because the cooling liquid remains in the same phase. This work presents an experimental study on the thermal performance of aluminum foam heat sinks in single-phase liquid immersion cooling (SPLIC). A set of heat sinks with varying pores per inch (PPI) and height is employed to test the thermal properties of heat sinks under different flow rates and power. Metal foams are used in place of conventional heat sinks for cooling, particularly aluminum alloy (Al-6101-T6) foam, which is a type of lightweight porous material with a cellular structure consisting of a large volume fraction of gas-filled open pores. It has a higher surface area-to-volume ratio, higher thermal conductivity, is lightweight, has increased turbulence, and has structural integrity at high temperatures. The goal of this experiment is to analyze the thermal and fluid properties of an aluminum foam heat sink when it is immersed in a synthetic dielectric fluid (EC-100). A customized tank was designed and fabricated for the experimental setup with a Thermal Test Vehicle (TTV), enabling the control of flow rate, heater temperature, and inlet temperature of the fluid. A set of experiments were conducted using aluminum foam heat sinks with varying pores per inch (5, 10, 20, and 40 PPI) for varying flow rates (1, 2, and 3 LPM) and heights (0.5 and 0.75 inches) with a relative density of 10~12%, mounted on a heater plate of heat flux 19 W/cm^2 and 23.8 W/cm^2 respectively. Major outcomes from the experiment were that the heat sink of 10 PPI exhibited the best heat transfer and lowest thermal resistance, while the heat sink of 5 PPI exhibited the highest "overall surface area efficiency" in all conditions. The heat transfer was increased from 0.5-inch-high to 0.75-inch-hight foam cores.

Keywords: (SPLIC) single phase liquid immersion cooling, Heat flux, Pores per inch (PPI), Heat Transfer, Forced Convection, Data center, Metal Foam.

LIST OF FIGURES

Figure. 1. The development trend of chip power consumption, heat flux density, and transistor counts in the past 20 years.

Figure. 2. Types of electronic cooling methods.

Figure. 3. Conventional Cooling Methods.

Figure. 4. Typical spray cooling curve (FC-72, 93 ml/min, ΔT_{sub} = 28 °C

Figure. 5. Schematic of Jet impingement Cooling.

Figure. 6. Schematic Single Phase Liquid Immersion Cooling.

Figure. 7. Schematic drawing of single-phase liquid immersion cooling setup immersed in coolant.

Figure. 8. Microchannel cold plate with equivalent thermal resistant model.

Figure. 9. Schematic Heat Pipe.

Figure. 10. Thermoelectric cooling concept.

Figure. 11. Working Principle of Vapor Chamber.

Figure. 12. PCM: The Melting/Solidification Process.

Figure. 13. Standard Heating Curve.

Figure. 14. Open-cell (Left) and Closed-cell (Right) metal foam structure

Figure. 15. Classification of process based on cell size and relative density of metal foam.

Figure. 16. Direct foaming of melts by gas injection.

Figure. 17. Direct foaming of melts with blowing agents.

Figure. 18. Production of metal foam by casting with polymer foams and space holder.

Figure. 19. Metal foam heat sink with open cell (Left) and closed cell (Right).

Figure: 20. Geometry of one cell (Tetrakaidecahedron) provided by Manufacturer (ErgAerospace).

Figure. 21. Aluminum Foam heat sink with 5,10,20, and 40 pores per inches (PPI).

Figure:22(A) Source: Duocell Geometry. Supplier: (ErgAerospace)

Figure: 22(B). Source: Duocell Geometry. Supplier: (ErgAerospace)

Figure:23. Thermal Test Vehicle (TTV)

Figure: 24. Metal foam core dimensions.

Figure:25. Thermal Test Chamber (EMNSPC UTA)

Figure: 26. Test setup CAD Design side view, isometric view and front view.

Figure: 27. Schematic Sketch of Thermal Test Vehicle.

LIST OF TABLES

Table: 1. Common coolants used in immersion cooling.

Table: 2. Fluid Properties of Dielectric Synthetic Fluid electro cool (EC-100)

Table: 3. Physical and Chemical Properties of EC-100

Table 4: Experimental Uncertainty

Table. 5. Specifications of Aluminum foam Heat sink. (Provided by manufacturer)

Table. 6. Specifications of Aluminum foam Heat sink. (Provided by manufacturer)

LIST OF GRAPHS

Graph:1. Thermal Resistance vs Flow Rate for Inlet Fluid temperature, Power, and Foam core height as 40°C, 200 Watts and 0.5 inch respectively.

Graph:2. Thermal Resistance vs Flow Rate for Inlet Fluid temperature, Power, and Foam core height as 40°C, 250 Watts and 0.5 inch respectively.

Graph:3. Local Heat Transfer vs Flow Rate for Inlet Fluid temperature, Power, and Foam core height as 40°C, 200 Watts and 0.5 inch respectively.

Graph:4. Local Heat Transfer vs Flow Rate for Inlet Fluid temperature, Power, and Foam core height as 40°C, 250 Watts and 0.5 inch respectively.

Graph:5. Overall surface area efficiency vs Flow Rate for Inlet Fluid temperature, Power, and Foam core height as 40°C, 200 Watts and 0.5 inch respectively.

Graph:6. Overall surface area efficiency vs Flow Rate for Inlet Fluid temperature, Power, and Foam core height as 40°C, 250 Watts and 0.5 inch respectively.

Graph:7. Global Heat Transfer coefficient vs Flow Rate for Inlet Fluid temperature, Power, and Foam core height as 40°C, 200 Watts and 0.5 inch respectively.

Graph:8. Global Heat Transfer coefficient vs Flow Rate for Inlet Fluid temperature, Power, and Foam core height as 40°C, 250 Watts and 0.5 inch respectively.

Graph:9. Thermal Resistance vs Flow Rate for Inlet Fluid temperature, Power, and Foam core height as 40°C, 200 Watts and 0.75 inch respectively.

Graph:10. Thermal Resistance vs Flow Rate for Inlet Fluid temperature, Power, and Foam core height as 40°C, 250 Watts and 0.75 inch respectively.

Graph:11. Local Heat Transfer (h) vs Flow Rate for Inlet Fluid temperature, Power, and Foam core height as 40°C, 200 Watts and 0.75 inch respectively.

Graph:12. Local Heat Transfer (h) vs Flow Rate for Inlet Fluid temperature, Power, and Foam core height as 40°C, 250 Watts and 0.75 inch respectively.

Graph:13. Overall Surface Area Efficiency vs Flow Rate for Inlet Fluid temperature, Power, and Foam core height as 40°C, 200 Watts and 0.75 inch respectively.

Graph:14. Overall Surface Area Efficiency vs Flow Rate for Inlet Fluid temperature, Power, and Foam core height as 40°C, 250 Watts and 0.75 inch respectively.

Graph:15. Global Heat Transfer vs Flow Rate for Inlet Fluid temperature, Power, and Foam core height as 40°C, 200 Watts and 0.75 inch respectively.

Graph:16. Global Heat Transfer vs Flow Rate for Inlet Fluid temperature, Power, and Foam core height as 40°C, 250 Watts and 0.75 inch respectively.

CHAPTER 1

1.1. Introduction

Microelectronics has evolved into the core of every contemporary electronic product, including advanced transportation, navigation, and energy management systems, as well as residential and office PCs. Nevertheless, the conversion of electrical energy to thermal energy is an inevitable consequence of the regular functioning of electronic devices, including microelectronic devices. This results in elevated temperatures within the microprocessor, which, if not effectively regulated, can have substantial detrimental effects on the performance, leakage power, and dependability of microelectronic chips, assemblies, and products.**[1]**. Sophisticated liquid cooling methodologies, including jet/spray cooling, microchannel cold plates, and liquid immersion cooling, offer exceptionally high heat transfer coefficients and may be employed to fulfill the aforementioned criteria **[2]**. Among the most promising enhanced surfaces are cellular materials that possess the following intrinsic multifunctional properties: a high heat transfer area to volume ratio, outstanding stiffness and strength, and enhanced flow mixing capability.

As a result, metal foams exhibit a diverse range of prospective uses in numerous industries, such as compact heat exchangers for airborne apparatus, air-cooled condensers for refrigeration and air conditioning systems, cryogenics, building cladding, strain isolation, petroleum reservoirs, and heat exchangers.**[3]**. Single-phase cooling is a method of sensible heating that utilizes circulating coolant in the absence of a phase transition. Water, by virtue of its exceptional thermophysical characteristics and elevated boiling point, stands as the most pragmatic coolant among the current array of refrigerants and dielectric fluids.

However, in the DCs industry, its utilization is of low priority and demand due to the potential for liquid leakage. **[4]**. With the introduction of a single package containing an integration of centrifugal pumps and cold plates, this limitation has been recently eliminated. This approach facilitates the liquid cooling of a series of processors while maintaining a high level of server dependability.

Numerous parameters influence the efficacy and thermo-flow characteristics of a single-phase water-cooling method; the effects of these parameters are exhaustively discussed in the literature. The primary objective of these investigations is to develop chip-level thermal management solutions via the design and testing of a variety of cold plates, including microchannel heat sinks and porous medium heat sinks. **[5]**, **[6]**, **[7]**. The literature extensively examines key parameters, including the pressure drop across the heat sink, the volumetric flow rate of the refrigerant, the temperatures at its inlet and outlet, the power supply required, and the heat transfer coefficient (HTC).

1.2. Power Consumption

Then, in the 1960s, in opposition to the rapid growth of the integrated circuit industry, the renowned "Moore's Law" was proposed. While "Moore's Law" is primarily an empirical relationship in production rather than a natural law, its validity has been established for decades, and it has been extensively applied in the semiconductor industry to guide research and development objectives. As illustrated in Fig. 1, the number of transistors that can be integrated into the circuit will continue to increase in accordance with Moore's law.

Concurrently, as market development demands increase, contemporary electronic devices undergo a process of miniaturization, resulting in increased thinness and lightness. A smaller device size and more transistors, on the other hand, result in increased power and thermal flux density.

Thus far, sophisticated server equipment processors have the capability to generate heat flux densities on the order of 1 MW/m^2. Furthermore, phased array radar and other equipment can achieve heat flux densities of 10-20 MW/m^2. In light of this, thermal management technologies are confronted with formidable obstacles in their quest to preserve operations within acceptable safety parameters. as determined by the US Air Force Avionics Integrity Program. Furthermore, Black's equation suggests that an elevation in temperature would hasten the deterioration of electronic components. As a result, addressing temperature concerns regarding electronic devices has gained significance in the present day. **[8].**

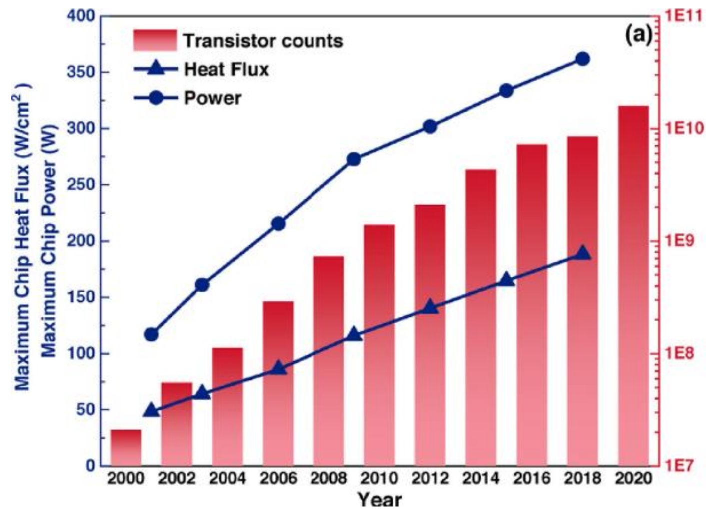

Figure. 1. The development trend of chip maximum power consumption, heat flux density, and approximate transistor counts in the past 20 years. **[9]**

CHAPTER 2

2.1. Types of Cooling Techniques

The following is a brief description of various electronic cooling techniques organized according to the type of contact.

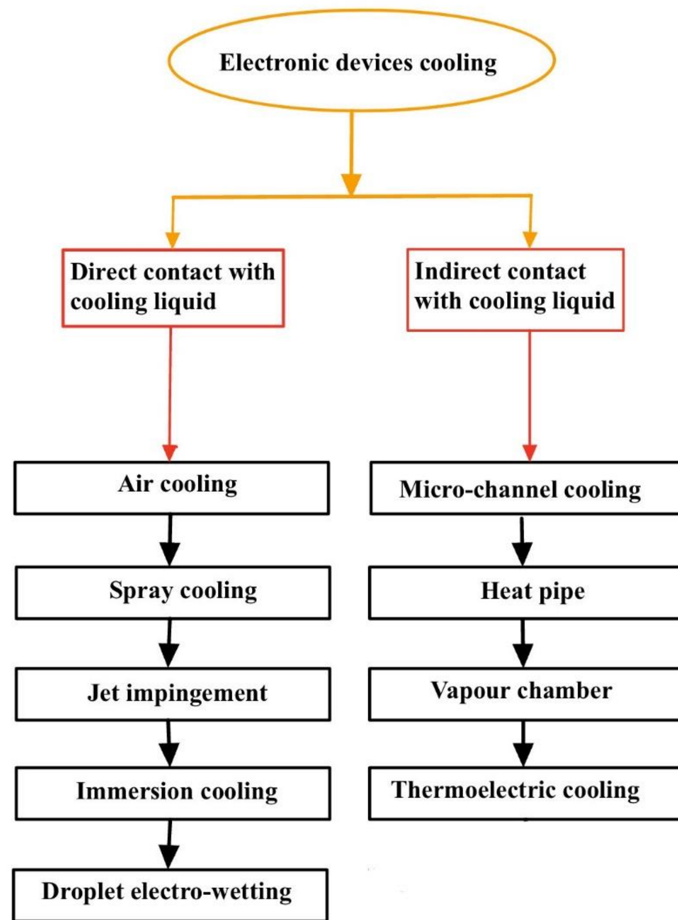

Figure: 2. Types of electronic cooling methods.

2.1.1.Direct contact liquid cooling

2.1.1.1. Air Cooling:

Implementing electronic thermal management through natural or free convection cooling is the most straightforward, practical, and cost-effective approach. **[10]** investigated the impact of

mounting angle on natural convection heat transfer in light of this. The straight-fin heat sink exhibits its most and least effective cooling capabilities when mounted at an angle of 15° and 90°, respectively. However, as illustrated in Figure 3, radiation and unrestricted convection are only advised for heat dissipation when the heat flux density is below 1550 W/m^2**[11]**. High-power electronic devices are thus more reliably cooled by compressed air or liquid. Two circumstances can be distinguished in terms of externally forced cooling in accordance with thermal management techniques. Initially, the cooling fluid (air or liquid) exerts a direct influence on the electronic device's surface. Subsequently, an intermediate heat absorber facilitates the dissipation of heat, thereby augmenting the heat transfer area and supporting the heat transfer process. Natural cooling research for electronic devices is currently quite scarce. **[12]**. The maturity of natural cooling as a technology for low-power electronics, such as televisions and VCRs, could account for this **[13]**, **[58]** For certain areas of thermal management, such as data centers, forced liquid cooling is essential (with or without phase change). The thermal management techniques utilizing liquid as the cooling medium will therefore be examined and discussed in depth in this thesis.

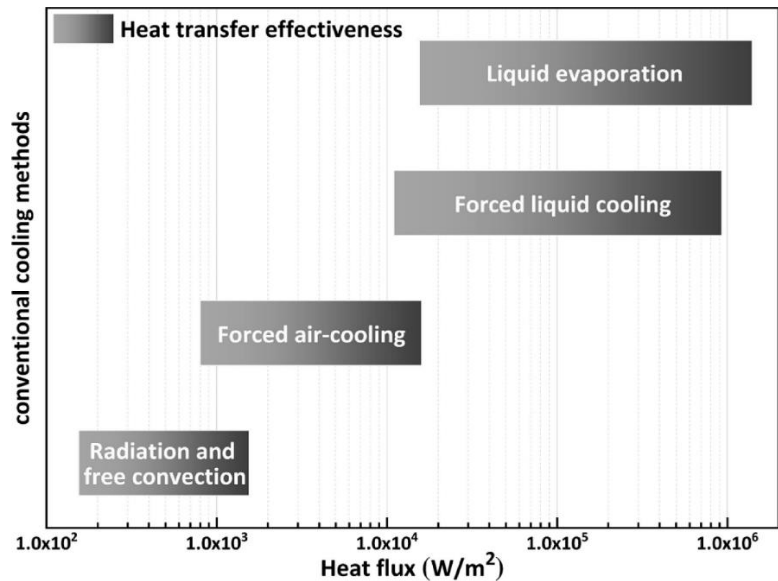

Figure: 3. Conventional Cooling Methods.

2.1.1.2. Spray Cooling:

Spray cooling is widely regarded as a highly efficient thermal management technique for high-power electronic devices owing to its substantial cooling area and capacity to dissipate a high heat flux. **[14]**. A nozzle is employed to decompress the cooling fluid into a multitude of minuscule

particles under intense pressure. The particles then exert a direct impact on the heated surface, thereby augmenting heat transfer. As shown in Figure 4, there are three phases to the practical spray cooling process, each of which has a different wall temperature. The initial phase is referred to as the single-phase regime. During this stage, the wall temperature remains within a relatively low range and increases nearly linearly; the cooling fluid undergoes no significant phase change. Then, as the surface temperature rises, the spray cooling is transferred to a two-phase regime, and the slope of the curve steepens considerably. Energy is required in significant quantities to enable the bubble nucleation process to surmount the energy barrier that promotes heat absorption. Additionally, the impact of particles induces agitation in the liquid film, which contributes to enhanced heat transfer performance. Finally, the heat flux will cease to increase once it reaches a particular critical value of surface temperature. Numerous parameters and factors can influence spray cooling. On the basis of the spatial configuration of the spray cooling system, these can be classified as heating surface properties, nozzle parameters, and cooling fluid characteristics. These parameters are interdependent through the mechanism of the spray cooling system.

Fewer flow rate requirements, greater heat dissipation capacity, reduced superheat, absence of temperature overshot, and absence of contact thermal resistance with the heating surface are a few of the numerous benefits of spray cooling. By utilizing spray cooling technology, electron devices demonstrated enhanced operational dependability at reduced temperatures. Spraying could decrease die (junction) temperatures by 33 °C and power consumption by 35% in comparison to air cooling. **[15]**. Despite the laboratory completion of real die reliability testing spray cooling's unquestionable applicability in high heat flux removal remains substantial.

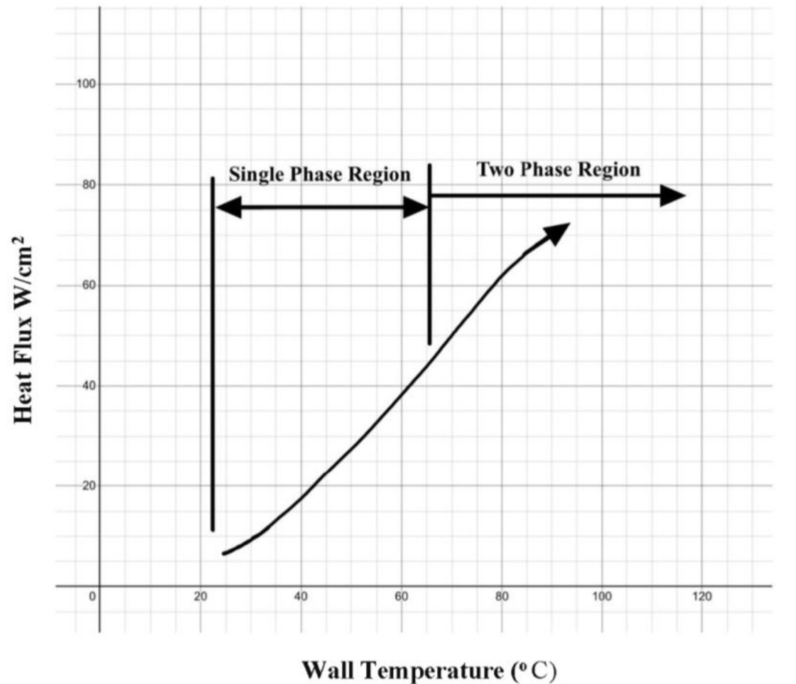

Figure: 4. Typical spray cooling curve (FC-72, 93 ml/min, ΔT_{sub} = 28 °C **[16]**

2.1.1.3. Jet impingement cooling:

Particularly in aerospace engineering and electronic cooling, where high heat fluxes are encountered, jet impingement cooling is an exceptionally efficient method for mitigating heat in a variety of engineering applications. To calm a surface, this method entails the guidance of a jet of fluid, which is commonly air or water. By propelling the fluid through a nozzle, which increases its velocity, a fluid jet is typically produced. Following that, the high-velocity fluid flow through impingement strikes the area that needs cooling. The fluid's impingement enhances heat transfer because of its increased momentum and turbulence. In jet impingement, convection and conduction are the principal mechanisms of heat transfer. Enhancing convective heat transmission, the impinging jet disrupts the boundary layer on the surface. Fluid Flow: Upon impact, the fluid disperses radially across the surface, which additionally facilitates the elimination of heat prior to its evacuation from the system.

Jet impingement shown in figure 5 has cooling performance substantially influenced by nozzle configurations and parameters. The extension of the jet hole **[17]**, could improve the heat transfer

process, eradicate misalignment of impinging areas, and mitigate the negative effects of crossflow. The impact of jet count, nozzle diameter, and configuration on cooling efficacy was investigated by **[18]** used numerical simulation to investigate the effects of jet count, nozzle diameter, and configuration on cooling efficacy. It was observed that marginal heat transfer could be enhanced with an increase in the number of jets.

However, this led to a corresponding rise in pumping power. Furthermore, minimizing the nozzle diameter improved heat transfer. Additionally, it was discovered by **[19]** that as the diameter of the nozzle increased, the heat transfer coefficient of jet impingement cooling diminished. Under the influence of severe cross-sections and whole flow field complexity **[20]** noted that the nozzle geometry and arrangement were responsible for determining the jet momentums under the influence of severe cross-sections and overall flow field complexity. The most effective cooling effect for jet impingement occurs in the central impinging region but falls precipitously as one moves away from this region.

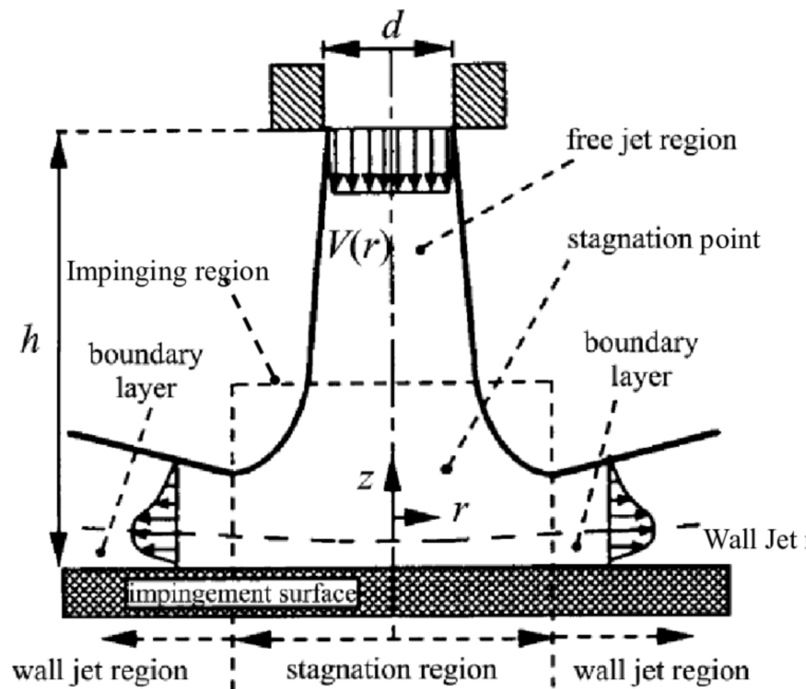

Figure: 5. Schematic of Jet impingement Cooling. **[20]**

2.1.1.4. Immersion Cooling:

One of the most efficient thermal management techniques is immersion cooling. In order to accomplish cooling, electronic devices are submerged in a dielectric fluid or coolant that possesses favorable thermal conductivity but prohibitive electric conductivity. Data centers**[21], [58]** and servers **[22]** have been extensively cooled utilizing immersion cooling. Combining immersion and spray cooling, **[23]** suggested a hybrid cooling technique. Comparing hybrid spray cooling to conventional spray cooling, they discovered that the former increased heat flux by as much as 65.6% under specific conditions. In a similar vein, **[24]** noted that immersion cooling of a natural convection-cooled fluid in motion could increase cooling efficacy by approximately 46%. Water is not utilized as a cooling fluid in numerous studies, as stated previously, because of its inadequate insulating properties in comparison to dielectric fluid. For both natural convection and nucleate pool boiling, water invariably possesses a higher heat transfer coefficient than dielectric fluid.

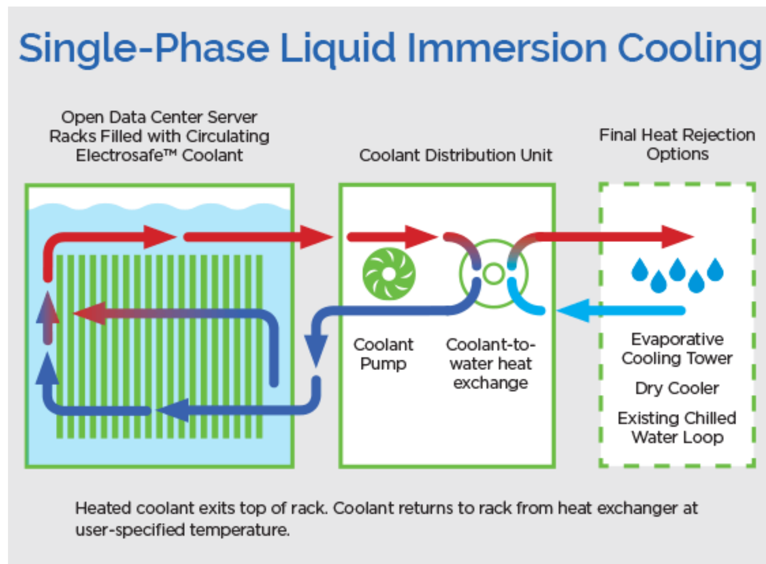

Figure 6: Schematic Single Phase Liquid Immersion Cooling.

Two-phase cooling, such as flow boiling, is hindered by hydrodynamic instabilities **[25]**, whereas single phase cooling is restricted to comparatively low heat transfer coefficients (2 kW/(m^2 K)) **[26]**. By facilitating the vaporization of a cooling fluid directly from electronic devices, immersion cooling has emerged as a potential solution to surmount these obstacles and the packaging restrictions that are associated with them. Modern SOA immersion cooling systems require non-conductive dielectric heat transfer liquids for electrical considerations, with the exception of the

use of treated, deionized water for certain systems. **[27]** Three fundamental disadvantages accompany the use of these fluids: (1) Electronic components are unable to significantly surpass the boiling temperature (~50 °C) of non-polar fluids at atmospheric pressure owing to the low boiling point. The crucial heat flux vapor blanket imposes this restriction. (2) In the context of next-generation high-power density systems, the critical heat flux of the working fluid determines the maximal heat flux achievable in the system. In the case of non-polar dielectric fluids, this flux is less than 20 W/cm^2, whereas it exceeds 100 W/cm^2 for such systems. Dielectric fluid doesn't have as good thermophysical properties as ideal conducting fluids like water. These properties include thermal conductivity, latent heat, and surface tension.

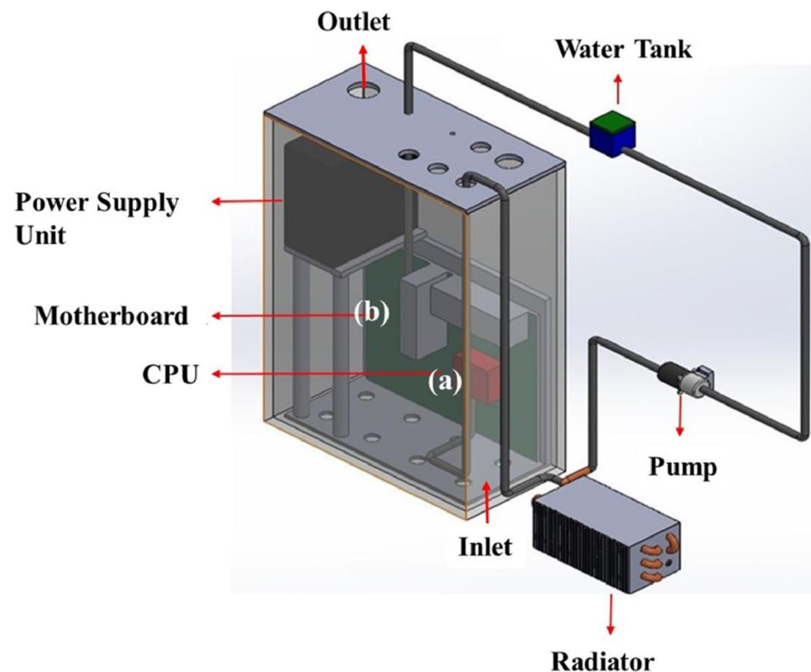

Figure: 7. Schematic drawing of single-phase liquid immersion cooling setup immersed in coolant. **[28]**

2.1.1.5. Droplet Electrowetting:

Droplet electrowetting, also known as electrowetting on dielectric (EWOD), is a method for altering the position and shape of a liquid droplet on a solid surface. By manipulating the moisture characteristics of the particle, this field enables meticulous regulation of its trajectory and

morphology. Significant implementations of this technique can be found in numerous disciplines, such as microfluidics and optical devices. Electrowetting operates on the principle that by applying a voltage, it is possible to alter the contact angle between a liquid droplet and a surface. At the point where the liquid, gas, and solid phases converge, the contact angle is measured. When an electric field is applied, the energy state of the system is altered, resulting in a modification of this angle.**[29]**. Extensive research has been conducted in the scientific and industrial communities on electrowetting, one of the most effective techniques for regulating droplet sheen. Gabriel Lippmann in 1875 first postulated electrocapillary, the fundamental principle underlying electrowetting. The Young-Lippmann equation, denoted as **[30]**, is a mathematical expression utilized to depict the correlation between the electric field effect and down-stream contact angle.

$$Cos\theta = Cos\theta_{eq} + CV^2/2\gamma$$

where θ_{eq} is the equilibrium contact angle for zero external voltage, and C is the capacitance/unit area, V is voltage and V^2 should change to ${V^2}_{eff}$ (effective voltage) for alternating-current electrowetting. There are currently an increasing number of electronic device thermal management applications involving droplet electrowetting. One such technology is EWOD (Electrowetting on Dielectric) **[31]**, which boasts several benefits, including rapid response, elimination of pressure drop, and minimal energy consumption.

2.1.2. Indirect contact cooling

2.1.2.1. Microchannel Cooling:

Microchannel cooling is a process that removes heat from electronic systems or components through the efficient circulation of a coolant through minute, intricately designed channels. Traditional cooling methods are insufficient for high-power electronic devices, where this technology is particularly vital. This paper extensively examines the design, implementation, and efficacy of the microchannels in question, with a particular focus on their capacity to augment heat transfer efficiency. By utilizing the increased surface area that the microchannels offer, these cooling systems effectively manage heat. As a result, they have become indispensable in

contemporary electronics and other domains that demand sophisticated heat dissipation solutions **[32]**.

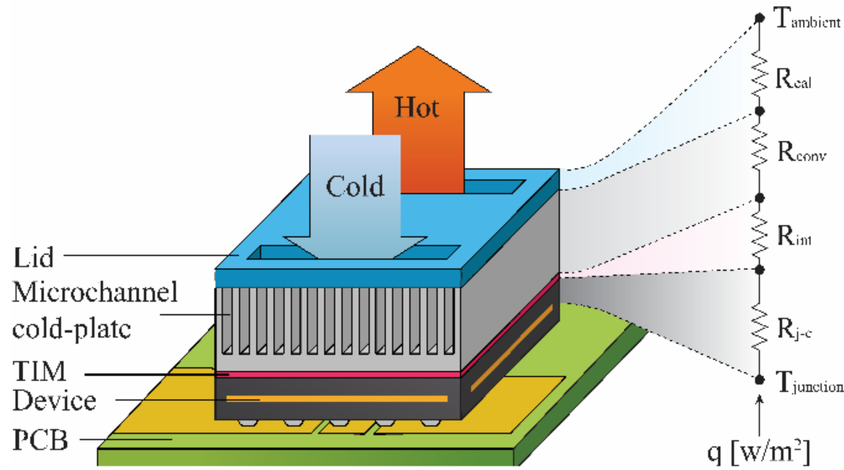

Figure 8: Microchannel cold plate with equivalent thermal resistant model.

The microchannel heat sink method was initially introduced by Tuckerman and Pease in 1981. The hydraulic diameter of microchannels was defined in **[33]** and **[34]** as varying between 1 and 100 µm and 10 to 200 µm, respectively. After optimization, the microchannel heat sink achieves improved temperature uniformity and a heat dissipation capability of over one thousand W/cm^2. A typical microchannel heat sink is utilized for the thermal management of chipsets. Researchers are becoming increasingly interested in microchannel cooling research, and the variables that may influence the capability of microchannel cooling have been the subject of extensive investigation. This section categorized research on microchannel cooling into two main aspects: microchannel structure and cooling fluid properties. The intention was to provide a comprehensive overview of the field of microchannel cooling research.

2.1.2.2. Heat Pipe Cooling:

As an innovative method of cooling electronic devices including satellite, computer, laptop, and telecommunication modules, heat pipes rely on the phase change of the working fluid within the pipelines. Heat pipes, which have an exceptionally low effective thermal resistance (typically ranging from 0.05 to 0.4 °C/W **[36]** and an exceedingly high effective thermal conductivity (up to

several thousand times higher than copper rod), are among the most practical methods for cooling electronic devices that generate high heat flux, including CPUs. Existing commercial applications for heat pipes as cooling devices are numerous, and the electronic industries have taken a keen interest in this method due to its exceptional heat removal capabilities. This is supported by the enormous quantity of heat pipelines manufactured in industry. As cooling systems for CPUs, laptops, and computers, for instance, millions upon millions of heat pipelines are produced monthly. Refrigerating laptop Pentium processors is, in fact, one of the most substantial uses of heat pipes. **[37]** recently published an extensive examination encompassing the design, fabrication, and performance evaluation of miniature heat pipes utilized in the cooling purpose of electronic devices. Additionally, they demonstrated how these diminutive heat ducts could be utilized to cool systems and electronic devices.

Heat pipes are of following types:

1.Flat heat pipes,
2.Cylindrical heat pipes,
3.Loop heat pipes,
4.Micro-heat pipes
5.Oscillating (also known as pulsating) heat pipes.

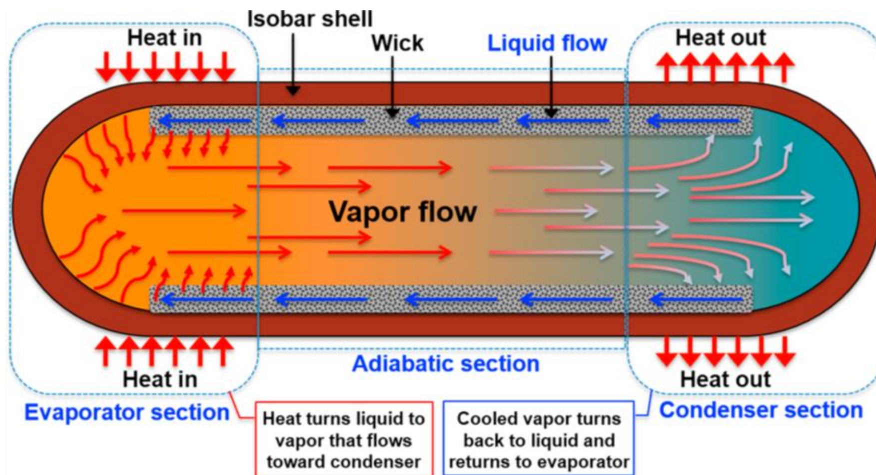

Figure 9: Schematic Heat Pipe.

2.1.2.3. Thermoelectric cooling:

Heat transfer occurs between the junctions of two distinct types of semiconductors via the Peltier effect, also referred to as the thermoelectric effect, when a thermoelectric cooler (TEC) is operational. These cooling devices are also referred to as thermoelectric coolers and Peltier heat pumps. By transferring heat from one side to the other, it requires the use of electrical energy. Due to their small size and lack of moving parts, TECs have the capacity to significantly improve the cooling rate of electronic modules and other electronic components **[38]**.

Additionally, TEC can be incorporated into electronic products to cool their hotspots. While the coefficient of performance of a thermoelectric cell (TEC) is comparatively lower than that of a vapor-compression refrigeration (VCR) system, Zebarjadi **[39]** established that for thermoelectric materials to be suitable for electronic cooling applications, they must possess high thermal conductivity and a large power factor. Saengchandr and Afzulpurkar **[40]** conducted an alternative investigation wherein they presented a numerical analysis of a heat pipe-based and combined thermoelectric module technology utilized to cool microprocessors and other computer circuits.

They asserted that the combined cooling system's temperature was lower than that of existing cooling systems and that its proposed cooling capacity was adequate for dissipating 200 W of heat.

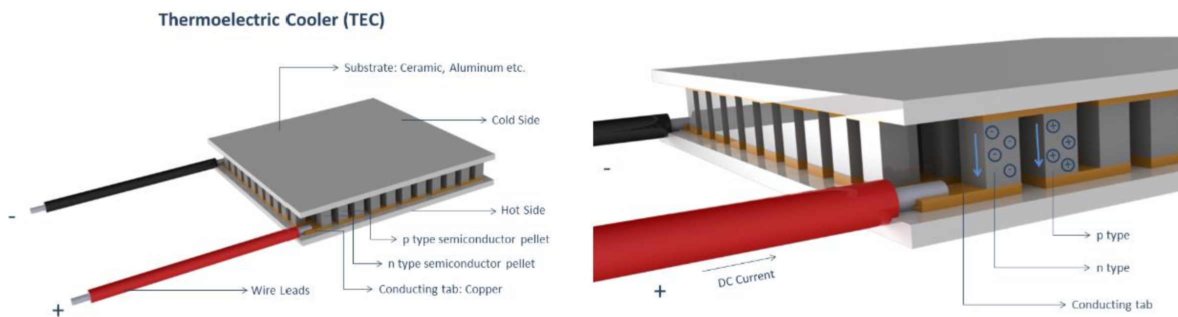

Figure 10: Thermoelectric cooling concept.

2.1.2.4. Vapor Chamber:

Vapor chamber cooling is a highly developed thermal management method that finds widespread application in applications involving high heat flux, including electronic cooling. By utilizing the principles of phase change and thermal conductivity, it dissipates heat in an efficient manner. A

grooved vapor chamber is typically positioned between a chilly plate and heat sources in a typical configuration. At the base of the vapor chamber, metal ceramic heaters (MCHs) are utilized to introduce heat into the system. The cooling water of the chilly plate ultimately extracts this heat after transferring it through the vapor chamber (VC). By facilitating efficient heat dissipation and distribution, this process renders vapor chambers exceptionally efficient in controlling the thermal burdens of compact and high-power electronic devices.**[41]**

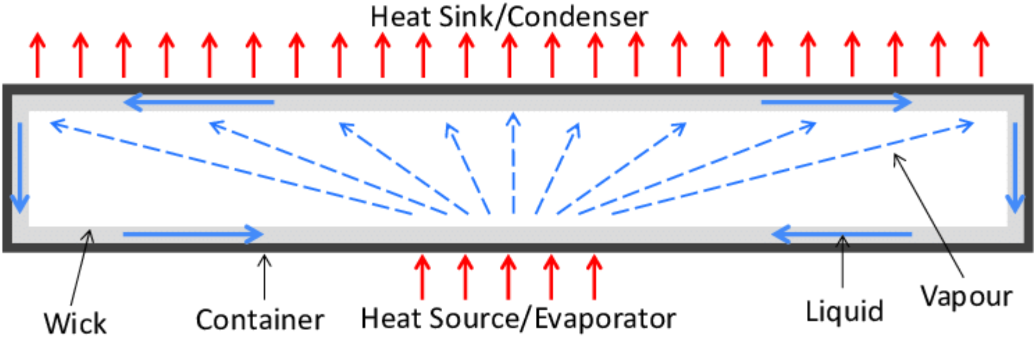

Figure 11: Working Principle of Vapor Chamber **[42]**

2.1.2.5. PCM Based Cooling:

PCM-based cooling has garnered significant interest in recent years as an emergent passive method. This cooling method exhibits great potential due to its ability to absorb heat from devices and appliances and store it for subsequent uses, including heating residential or commercial spaces. PCMs **[43]**, which possess a multitude of benefits such as a high specific heat, a high latent heat of fusion, and the ability to regulate temperature stability while undergoing phase changes, have been extensively investigated for a wide range of applications, including the cooling of electronic devices **[44]**. Phase transition materials (PCMs) have the ability to absorb substantial amounts of heat without experiencing an increase in temperature.

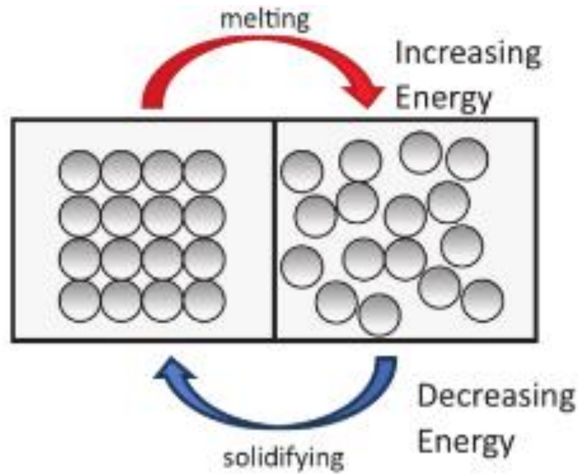

Figure 12: PCM: The Melting/Solidification Process. **[43]**

Jaworski and Domanski **[45]** proposed a novel microprocessor cooling heat sink design incorporating PCM. The authors conducted a numerical analysis to examine the thermal characteristics and performance of this design. They demonstrated that a small amount (mass) of PCM in the heat sink can substantially enhance its ability to stabilize the temperature of the microprocessor, indicating that PCM-based heat sinks have great potential for cooling electronics. Figure 8 illustrates the schematic design of a basic heat sink composed of PCM.

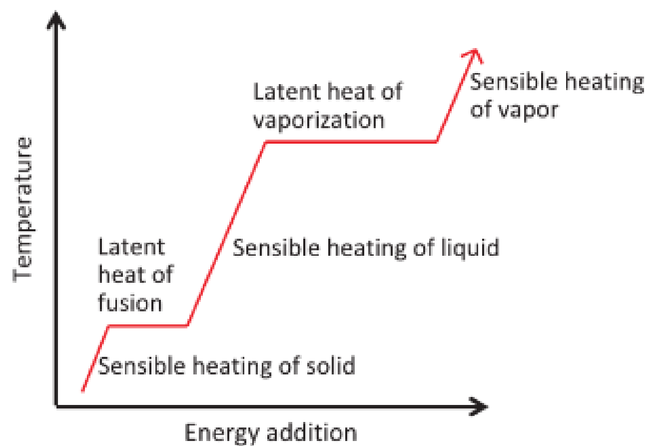

Figure 13: Standard Heating Curve**.[45]**

CHAPTER 3

3.1. Coolant Fluids

By submerging electronic components in a non-conductive liquid coolant that absorbs heat directly from them, single-phase liquid immersion cooling is a technological process. In high-power density applications, such as data centers and battery thermal management systems, this method is becoming more prevalent due to its efficacy. Single-phase liquid immersion cooling is dependent on the following coolants for optimal performance.

(1). Di-electric fluids, characterized by their exceptional thermal properties and chemical stability, are frequently employed in various applications. They are incapable of causing electronic component damage or brief circuits.

(2). Engineered fluids, which are environmentally benign and have been purposefully engineered to facilitate cooling, possess exceptional thermal conductivity and capacity. However, their cost exceeds that of conventional coolants.

(3). Mineral lubricants are frequently utilized for single-phase liquid immersion cooling due to their low cost and high thermal stability. Conversely, they might necessitate supplementary attention to handling and maintenance.

It is critical to choose the optimal refrigerant for a given cooling system or device. Coolant specifications are subject to variation based on the specific cooling systems and electronic devices in use. As is common knowledge and extensively discussed in the scientific literature **[46]**, **[47]**, liquid coolants utilized in electronic devices must possess exceptional thermophysical properties and characteristics, including low viscosity, high thermal conductivity, specific heat, and heat transfer coefficient, in addition to being non-combustible and inexpensive.

In addition to possessing favorable chemical and thermal stability, coolants must also exhibit compatibility (e.g., non-corrosiveness) with the constituent materials of both the devices and the cooling systems. Furthermore, a low freezing point, a high flash point, a boiling point, and an auto-ignition temperature are desired. Notably, heat transfer characteristics alone are insufficient when

selecting a coolant for direct immersion cooling. Additionally, the coolant's chemical compatibility with the electronics and other packaging materials must be evaluated.

3.2. Coolants used in immersion cooling.

Due to its superior thermal conductivity, specific heat, and reduced viscosity in comparison to alternative coolants, water is the coolant of choice for electronic devices. However, due to its high freezing point and subsequent expansion upon chilling, water is not utilized in closed-loop systems.

Fluids	Thermal conductivity. (W/m.k)	Cooling Mechanism	Boiling point (^{0} C)
Ethanol	0.167	Two Phase	78
Water-ethylene glycol	0.37	Single/Two Phase	107.3
Mineral oil	0.13	Single Phase	150~200
Novac 649	0.059	Two Phase	49
Novac 7000	0.075	Two Phase	34
FC-3283	0.066	Single Phase	128
FC-43	0.065	Single Phase	178
FC-72	0.057	Two Phase	56

Table: 1. Common coolants used in immersion cooling.

3.3. Dielectric synthetic Fluid (EC-100)

Electro Cool EC-100 is an electrical component cooling heat transfer fluid. It is composed of a biodegradable, benign synthetic hydrocarbon. Single-phase liquid synthetic dielectric coolant utilized for pressure compensation. lubrication and power transmission in applications involving water. Extremely low aquatic toxicity and biodegradability. Designed for Liquid Immersion Cooling of Electronics in a Single-Phase Servers, GPUs, FPGAs, and other semiconductors operate in ever-smaller packages and at ever-increasing energy densities.

EC-100				
Temperature (^oC)	**Dynamic viscosity. (kg/m-sec)**	**Density (Kg/m^3)**	**Thermal conductivity (W/m. K)**	**Specific heat (KJ/kg. K)**
20	0.021	845.8	0.139	2.131
25	0.017	842.5	0.138	2.15
30	0.014	839.2	0.1378	2.16
35	0.012	835.9	0.1377	2.18
40	0.01	832.6	0.1374	2.20
45	0.008	828.7	0.1370	2.22
50	0.007	826	0.1366	2.24

Table: 2. Fluid Properties of Dielectric Synthetic Fluid electro cool EC-100 (by supplier)

Dielectric Electro cool EC-100 has specialized cooling fluid properties in other applications where direct contact with electrical components is necessary. Its key properties are based on its design to be non-conductive and chemically stable, making it suitable for use in environments were traditional cooling methods, like water or air, would be problematic.

Property	Value
Appearance:	Clear
Odor:	Slight
pH:	Not applicable
Freezing point (°C):	-65
Initial boiling point and boiling range (°C):	>350
Flash point (ASTM D92, °C)	190
Upper/lower flammability or explosive limits:	Data not available
Vapor pressure @ 20C, kPa	0.01
Vapor density:	Not applicable
Relative density at 20°C.:	0.8
Water solubility (ppm):	<80ppm
Partition coefficient:	>4.82@20C
Auto-ignition temperature (C):	>350
Decomposition temperature:	N/A
Kinematic Viscosity, cSt @ 40 °C:	8.1
Explosive properties:	Non-explosive
Oxidizing properties:	Non-oxidizing

Table: 3. Physical and Chemical Properties of EC-100 **[48]**

CHAPTER 4

4.1. Metal Foam

Metal foam: Metal foam is a form of porous, lightweight material composed of metal. It is predominantly composed of gas-filled cavities within a metallic matrix that comprises a significant portion of its volume. These pores may be open-cell or closed-cell; in closed-cell foams, the gas is confined to regions within the material, whereas in open-cell foams, the pores are interconnected. They possess a number of advantageous characteristics for thermal management solutions, including low weight, a large surface area, a high strength-to-weight ratio, efficient energy absorption, elevated thermal conductivity, an improved heat transfer coefficient, and excellent permeability.

Metal foam is of two types in terms of geometry:

4.1.1. Open-Cell Metal Foams

Open-Cell Metal Foams, Geometry: Open-cell metal foams have pores and cells that are interconnected to form a network that allows fluid to move through it. The cell walls are typically quite thin, and the structure is very similar to that of a sponge.

4.1.2. Closed-Cell Metal Foams

Closed-Cell Metal Foams, Geometry: Metal foams with closed cells have their pores hermetically shut and filled with gas. The cells in closed-cell foams are not connected to one another in the same way that they are in open-cell foams. Because of its structure, the final product has increased strength and stiffness relative to its weight.

At the present point in time, the vast majority of metal foams that are commercially available are either based on aluminum or nickel. There are processes that can be used to foam magnesium, lead, zinc, copper, bronze, titanium, steel, and even gold, and these processes are accessible on demand. Because of the amount of effort put into research and the development of new processes, it is projected that the variety of foams that are commercially available will grow at a rapid rate over the course of the next five years.

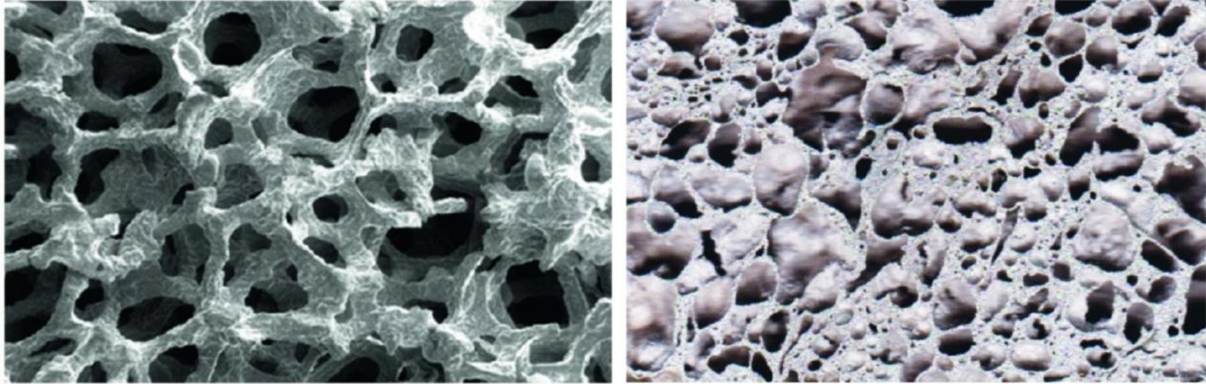

Figure: 14. Open-cell (Left) and Closed-cell (Right) metal foam structure

4.1.3. Applications:

Lightweight structures	Excellent ratio of stiffness to weight when applied in the bending direction
Sandwich cores	Metal foams have a low density while maintaining excellent shear and fracture strengths.
Thermal management in heat exchangers	Open-cell foams are exceptional refrigerators due to their large accessible surface area heat exchangers and high cell-wall conduction.
Energy management:	The capacity of metal foams to absorb condensed or light energy at nearly constant pressure is extraordinary.
Thermal management:	Cell margins with a high thermal conductivity are combined with flame arresters.
Buoyancy	Low density and excellent corrosion resistance indicate potential for use in floatation applications.

Electronic Cooling	Effective thermal management is essential for preserving performance and dependability.
Energy Absorption and Dissipation	Due to their porous structure, metal foams are capable of efficient energy absorption.
Refrigeration Systems:	Metal foams have the potential to increase the efficacy of heat exchangers in refrigeration, resulting in systems that are more compact and efficient.
Consumable cores for Met foams, injection	Molded into intricate configurations, castings serve as consumable cores for aluminum castings.

4.2. Making of Metal Foams:

Phase dispersion and pore morphology exhibit certain distinctions. The following are some such distinctions **[49]**:

(a) **Metal foam** - A diverse array of cells is present. A cell is open if it is situated in close proximity to the membrane cell that separates it from the adjacent cell. The designation ‘metal foam' is exclusively applied to hollow metals produced through the dispersion of the gas phase within the solid metal.

(b) **Porous metal** - Spherical cell units are present. Isolated, separated, and coarse cells are produced. In general, total porosity falls below 70%. The designation "porous metal" is applied to metals or solid substances in which the hollow metal is not generated through the dispersion of gas phases.

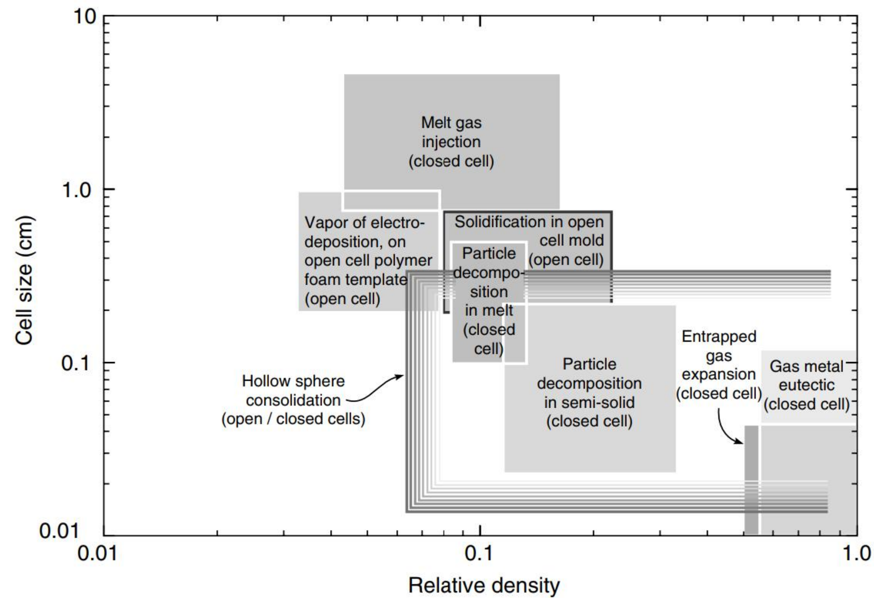

Figure:15. Classification of process based on cell size and relative density of metal foam.

The most prevalent technique, liquid-state processing, is appropriate for metals and metal alloys that possess a low melting point. Foaming of liquid metals can be achieved via direct foaming or indirect processes, including casting onto polymer foams. The following techniques are classified as liquid processing methods:

(1). Foaming by gas injection

(2). Foaming with blowing agents

(3). Solid–gas eutectic solidification (‘gasars’)

(4). Casting methods

(5). Powder compact melting technique.

4.2.1. Foaming by Gas Injection

This technique is pioneering in its application to aluminum foams. Melts are depicted in the figure as foaming due to gas injection. In order to produce molten metal, the metal is heated to its melting point. The molten metal is subsequently infused with binder and stabilizer substances, including silicon carbide and aluminum oxide. Injecting gas into the molten metal to create a gas pocket is the next step. Gas injection can be accomplished through the utilization of a rotary or vibrating nozzle that is specifically engineered to deliver air, nitrogen, or argon. As the gas droplets ascend

to the surface of the molten metal, they will coalesce into metal foams. **[52]**. The metal foams formed will be drained out by the conveyor belt as shown in Figure. **[54]** emphasized that in order to achieve the desired thickness and density, process parameters, including gas injection pressure, conveyor speed, and nozzle vibration frequency, must be precisely regulated. This method is capable of producing vast quantities of porous metal foams. Nevertheless, this material exhibits certain limitations, including toughness in regulating pore morphology and incompatibility with exceedingly reactive metals, like titanium.

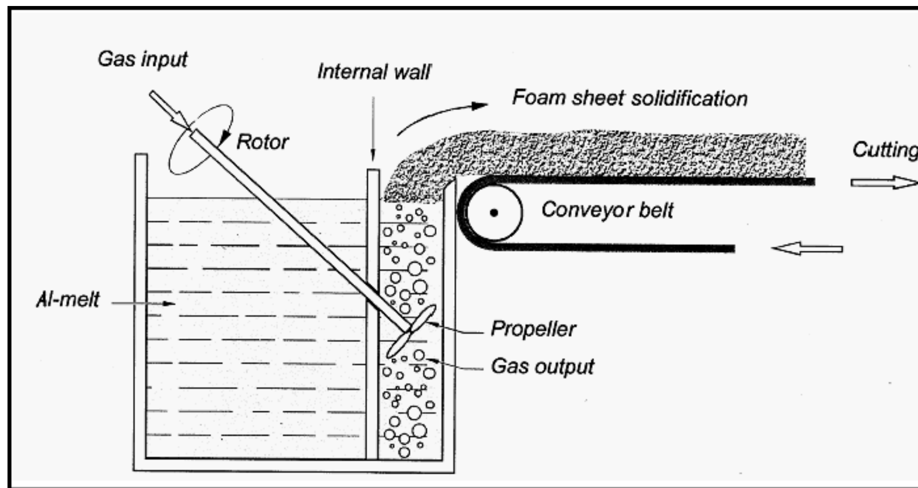

Figure:16. Direct foaming of melts by gas injection **[53]**.

4.2.2. Foaming with Blowing Agents

Rather than employing gas blowing, metal alloys can be foamed directly using a blowing agent. When heated, blowing agents decompose into gas that foams the molten metal. This method was devised and patented in 1986 by Shinko Wire Company, Ltd. In **[55]** With forcing agents, the foaming process is illustrated in Figure. This procedure begins with aluminum dissolving at 680 degrees Celsius. Calcium is infused with molten aluminum in order to increase its viscosity. Due to its high electron affinity, calcium is capable of thickening liquids by forming calcium oxide and calcium-aluminum oxide. Following this, titanium hydride (TiH2), which serves as a blowing agent, is introduced into the molten material. The hydrogen gas produced when titanium hydride decomposes will cause the molten material to expand and fill the mold. Once the aluminum foam block has cooled, it is extracted from the mold and the production process is repeated. The duration of the entire procedure is approximately 15 minutes. The metal foams generated through this

process are commercially known as ALPORAS [**54]** Although this technique can rapidly generate foam that is relatively homogeneous, it is challenging to regulate the pore size and shape.

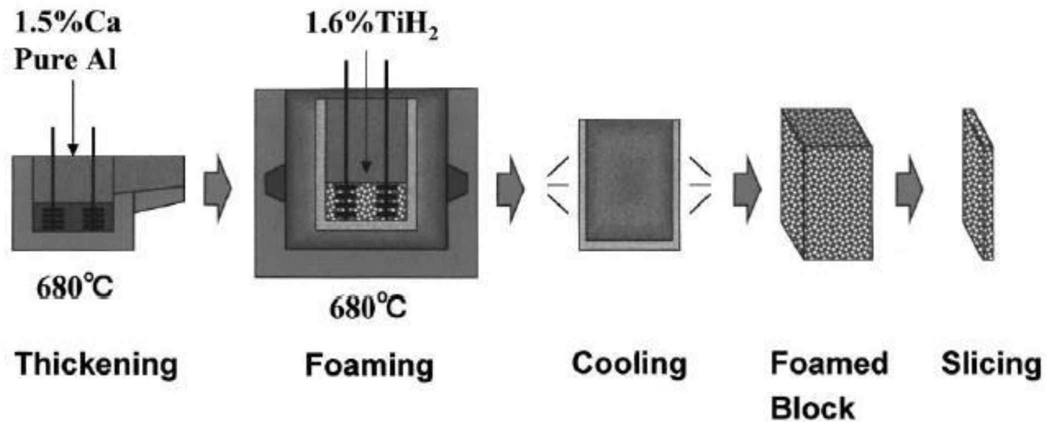

Figure: 17. Direct foaming of melts with blowing agents **[56]**.

4.2.3. Solid–gas Eutectic Solidification (Gasars).

Certain liquid metals, including magnesium, copper, and aluminum, form eutectic systems with hydrogen gas. As a result, this technique was devised. When liquid metal is heated in an atmosphere of high-pressure hydrogen, a two-phase eutectic system is formed, consisting of hydrogen gas and a charged dissolve. The hydrogen gas is absorbed by the liquid metal during cooling and solidification, resulting in the formation of cavities within the metal. This technique is referred to as GASAR, an acronym that translates to "gas-reinforced porous material" in Russian. The hydrogen gas content, gas pressure over the liquid, cooling rate, and chemical composition of the molten metal all influences the pore morphology. Pores are generated in the form of elongated, solidification-oriented pores. Continuous casting is compatible with this technique in 2012 according to **[54]** This method is incapable of producing metal foams with a uniform pore size distribution.

4.2.4. Casting Methods

Methods of casting are indirect forms of liquid-state processing. Metal foams can be cast by researchers using polymer foams or space holders. The illustration depicts metal being cast using polymer foam. A high-temperature-resistant slurry is injected into polymer foam. Once the

polymer foam has dried, it is eliminated via thermal treatment. By then, a molten metal had been infused into the newly formed mold. The mold is filled with molten metal and is subsequently extracted once it has cooled. The procedure for casting the material of the space holder is illustrated in Figure 18. Typically, space holders are composed of particulate organic or inorganic materials. Following the space holder has been positioned in close proximity to the mold, the molten metal is then poured into the mold. Following the cooling and solidification process, the filler material is extracted via solvent application or thermal treatment. Pore morphology can be easily modified through adjustments to the space holder's dimensions and configuration. However, this approach continues to be unsuitable for highly reactive metals, such as titanium.

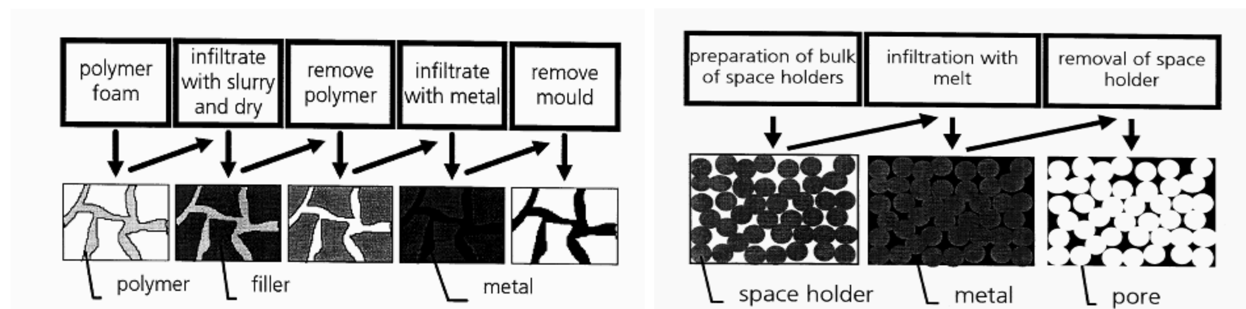

figure: 18. Production of metal foam by casting with polymer foams and space holder F **[54]**

4.2.5. Powder Compact Melting Technique

This method was devised by the Fraunhofer-Institute in Bremen, Germany **[54]** In this procedure, metal powder is employed as the initial step. Although frothing occurs during the process of melting, it is still categorized as production in the liquid state. The metal powder is initially incorporated with the dispersing agent. Extrusion or compression is used to compact the mixture. **[57].** A heat treatment is conducted at or in the vicinity of the metal's melting point to promote the blowing agent's decomposition. The formation of fissures in the molten metal will result from the component expansion induced by the discharged gases. The adjustment of expanding agent composition and type can result in a modification of the density of metal foams. However, this methodology is not capable of controlling the pore morphology and is not feasible for metals with a high melting point as a result of the prohibitive processing costs.

4.3. Characterization

(A). Based on cell structure:

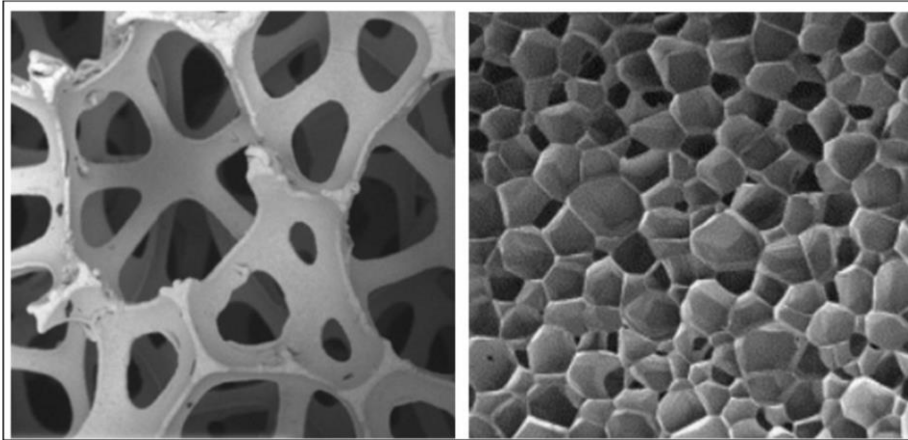

Figure:19. Metal foam heat sink with open cell (Left) and closed cell (Right).

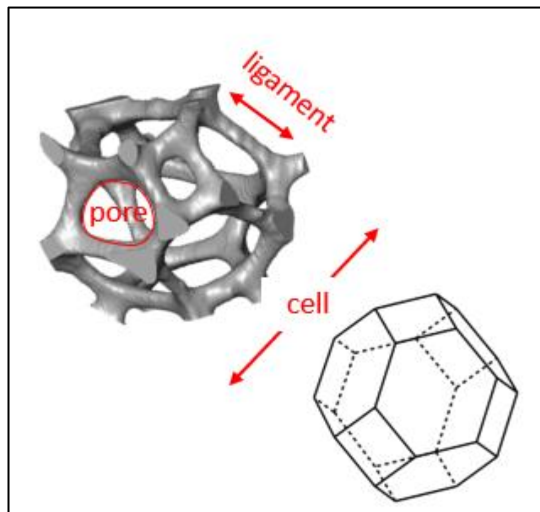

Figure: 20. Geometry of one cell (Tetrakaidecahedron) provided by Manufacturer (ErgAerospace).

(B). Based on pores per inches:

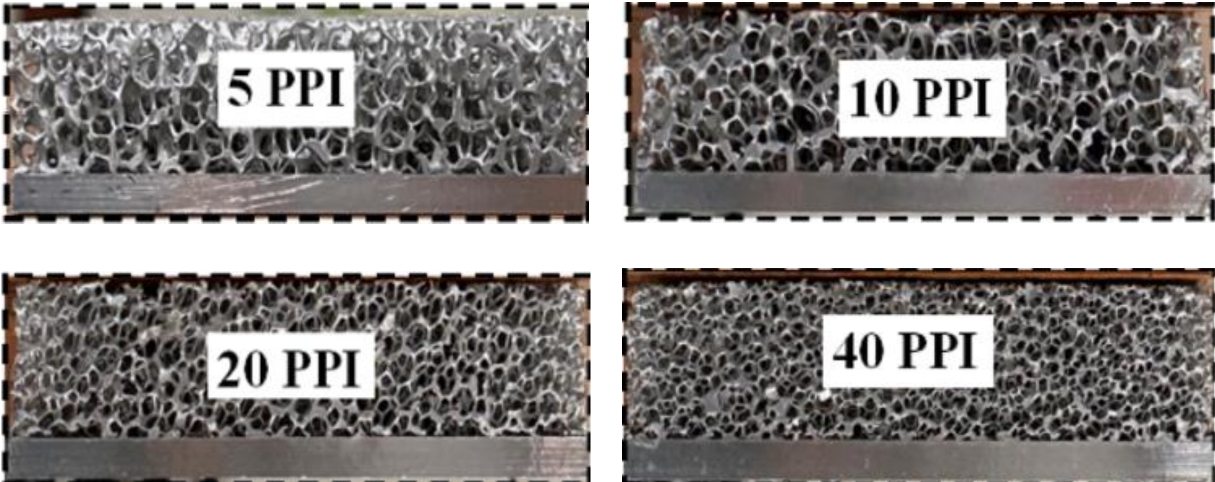

Figure:21. Aluminum Foam heat sink with 5,10,20, and 40 pores per inches PPI (ErgAerospace).

(C). Based on Ligaments arrangement:

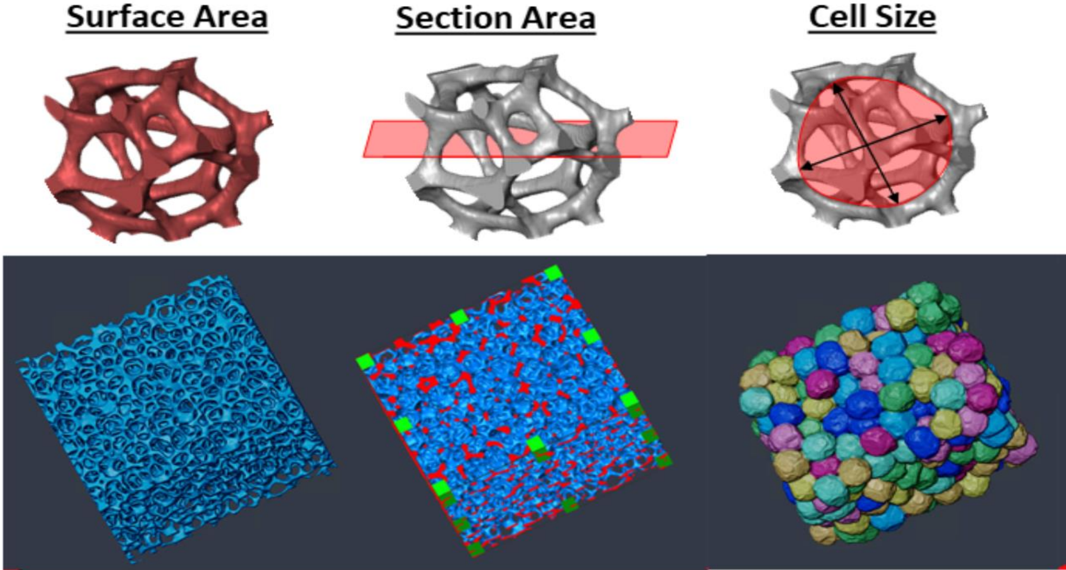

Figure:22(A) Source: Duocell Geometry. Supplier: (ErgAerospace)

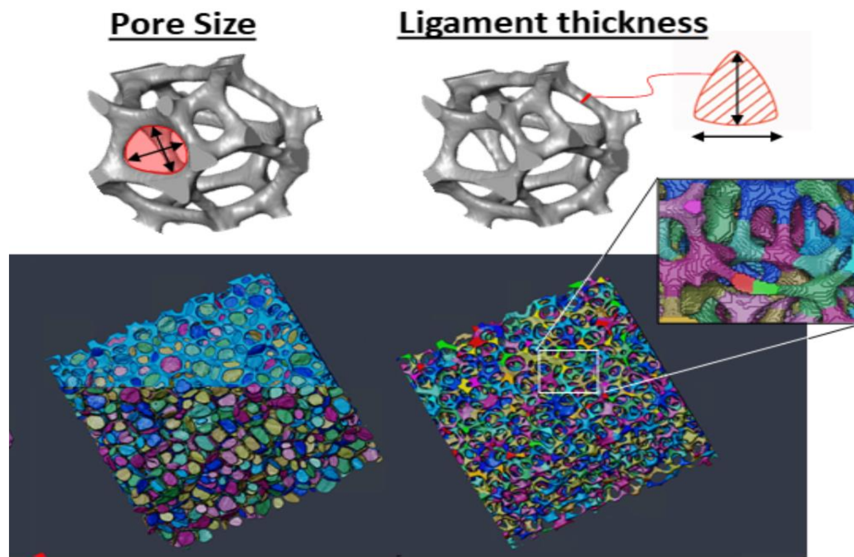

Figure: 22(B). Source: Duocell Geometry. Supplier: (ErgAerospace)

CHAPTER 5

5.1 Boundary Conditions:

- PPI: 5,10, 20 and 40
- Height: 0.5~0.75 inch
- Heat flux: 19 W/cm^2 and 23.8 W/cm^2.
- Flow rate: at 1, 2 and 3 LPM (Velocity: 174, 348, and 523 ft/sec respectively.)
- Inlet Temperature: 40°C

5.2 Data reduction:

The experimental data allow the total heat transfer coefficient HTC^* to be calculated by equation:

$$Q = \eta_o \times A \times \Delta T \times h = HTC^* \times A_b \times \Delta T \quad (1)$$

Where Q is the power, η_0 is overall surface area efficiency, A is the total heat transfer area, h is local heat transfer coefficient.

$$\Delta T = T_s - T_{avg\ fluid},\ T_{avg\ fluid} = \frac{(T_{outlet\ fluid} + T_{inlet\ fluid})}{2} \quad (2)$$

k_e the effective thermal conductivity can be get from expression 2 (Sadeghi et al., 2011).

$$k_e \approx \frac{1}{3}(1-\varepsilon)k_s \quad (3)$$

where (ε) porosity, which is relative density, k_s is the Metal foam thermal conductivity. The thermal resistance (R_{th}) can be calculated by:

$$R_{th} = \frac{T_s - T_{inlet\ fluid}}{Q} \quad (4)$$

When the flow through the metal foam is taken into consideration, the experimental pressure drop calculation can be discussed by using equation 4 (Bhattacharya et al., 2002). This is a pressure drop gradient in a rigid porous media equation that is widely accepted by the scientific community.

$$-\frac{dP}{dz}\frac{1}{u} = \frac{\mu}{K} + \frac{\rho\ f\ u}{\sqrt{K}} = A + \rho.C\ .u = A + B.u \quad (5)$$

The first term, denoted by the letter A, is the Darcy term, which is responsible for explaining the linear dependency of pressure drop on flow velocity at low mass flow rates. The inertia constant

is denoted by the letter B. According to Darcy's Law, the permeability (K) of the metal foams is the measure of the flow conductance of the matrix. The density of the fluid is denoted by the symbol ρ, the form coefficient is denoted by C, the average velocity is denoted by u, and the inertia coefficient f is contingent upon the internal structure of the foam. Equations 5, 6, and 7 can be used to determine the parameters of the fins, as well as the efficiency of the fins and the overall surface area efficiency.

$$m = \sqrt{\frac{HTC^{*} \text{ x } a_f}{k_e}} \tag{6}$$

$$\eta_f = \frac{Tanh\ (mH)}{mH} \tag{7}$$

$$\eta_0 = 1 - \frac{A_f}{A}\ (1 - \eta_f) \tag{8}$$

$$A = A_f + A_b + A_c \tag{9}$$

$$A_c = (1 - \varepsilon) \times A_b \tag{10}$$

$$A_f = L \times B \times H \times a_f \tag{11}$$

where A_f is foam surface area, a_f is the foam area\ unit of volume**,** A is the total heat transfer area, A_f is the base area of the heat sink, h is the local heat transfer coefficient, k_e is the effective thermal conductivity and H is the height of the foam core

5.3 Uncertainty Analysis:

Errors in the implementation of experimental methods and measurements are unavoidable. As a result, an uncertainty analysis must be performed to verify the precision and dependability of the findings. An element of uncertainty exists in every experimental instrument prior to, during, and subsequent to measurements. Experimental procedures and measurements are susceptible to error at all times. As a result, an uncertainty analysis must be performed to verify the precision and dependability of the findings. An element of uncertainty exists in every experimental instrument prior to, during, and subsequent to measurements. In this investigation, the following variables are susceptible to experimental uncertainty: power, temperature, flow rate, and pressure drop. Table 2 displays the uncertainty parameters that were ascertained through the implementation of calibration techniques. Using equation 10, the uncertainty regarding the heat transfer coefficient is computed.

$$\frac{\delta h}{h} = \sqrt{(\frac{\delta V}{V})^2\ + (\frac{\delta I}{I})^2\ + (\frac{\delta T_s}{T_s - T_{in}})^2\ + \text{calculated}} \tag{12}$$

In conclusion, the error assessments determined that the average uncertainty for the heat transfer coefficient, pressure gradient, and thermal resistance is 5%, 1%, and 1% correspondingly.

Parameters	Uncertainty Values
Flow sensor	0.2%
Pressure sensor	0.2%
K type thermocouple	± 0.5°C
10kΩ thermistors	±0.3°C
Power meter	±0.13% of the reading

Table 4: Experimental Uncertainty

CHAPTER 6

Experiment Setup:

This section describes the various elements comprising the experimental configuration depicted below. The primary loop comprises a coolant distributing unit (CDU) that is connected to the facility's cold-water supply and return lines. PG 25 is the coolant utilized in the CDU for the main loop. The second half of the experimental configuration contains an acrylic box that serves as housing for the thermal test vehicle. EC 100 is utilized as the coolant for the secondary loop. Using 10k thermistors and Keyence GP-M010 pressure gauges, the temperatures and pressures at both the inlet and the outlet are monitored, respectively, while the water flow rate throughout the tank is determined using Keyence clamp-on microflow sensors (Keyence FDX-A1). Between 5 and 20 mA is the corresponding output signal of the flow and pressure sensors. In order to store the experimental data, every sensor is calibrated and linked to the information acquisition device (DAQ Agilent 37940A).

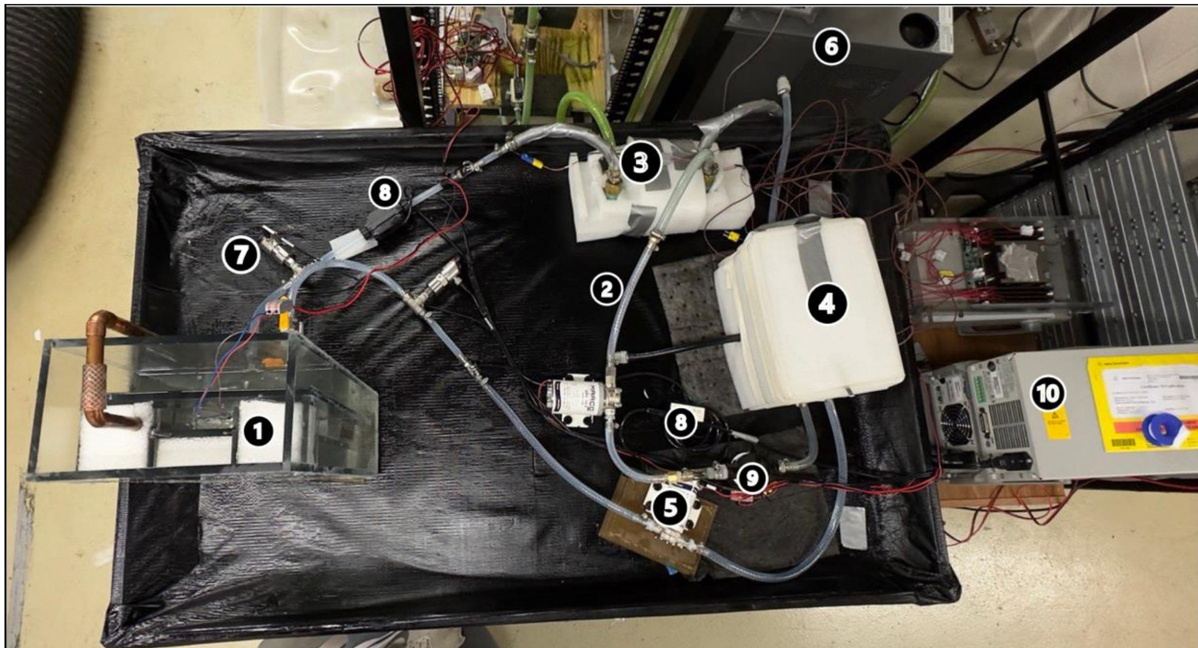

Figure:23. Thermal Test Vehicle (TTV)

1. Test vehicle chamber.

2. Connecting hose pipes.
3. Heat exchanger
4. Reservoir.
5. Pump
6. PolyScience chiller (liquid to liquid) **33kW @ 40°C** cooling capacity.
7. GP M010 pressure sensor (inlet and outlet).
8. Micro flow sensor (Clamp on and display).
9. Coolant Filter.
10. DAQ and power supply.

The experimental TTV consists of an insulating plate positioned at the bottom, upon which the heating element and the metal foam heat sink assemblage are affixed. the foam sample, which measures 3" x 3.5" x 0.5", and 3" x 3.5" x 0.75", is brazed to a 5mm-thick aluminum plate. A groove on the surface of the aluminum nitrite heater contains a K-type thermocouple, which is utilized to determine the surface temperature of the heater. Indium foil is utilized as thermal interface material (TIM), and an 8-pound torque is applied to the spring retention device of the heat sink.

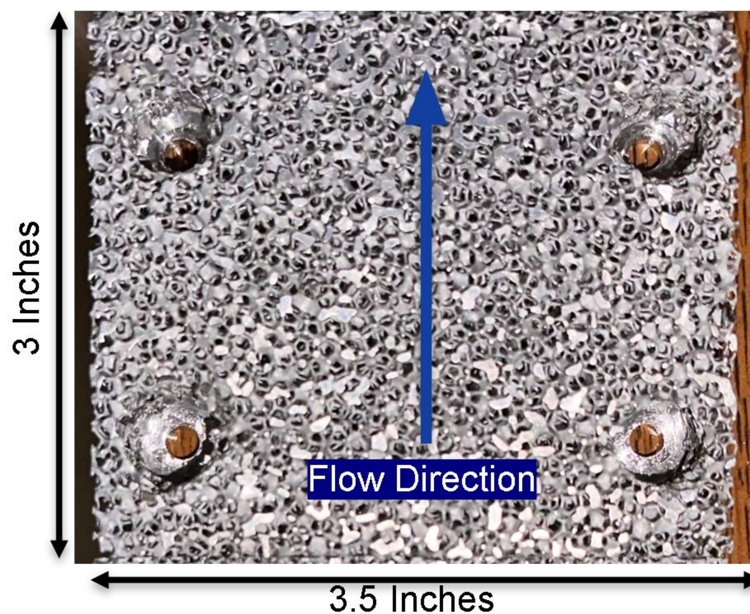

Figure: 24. Metal foam core dimensions.

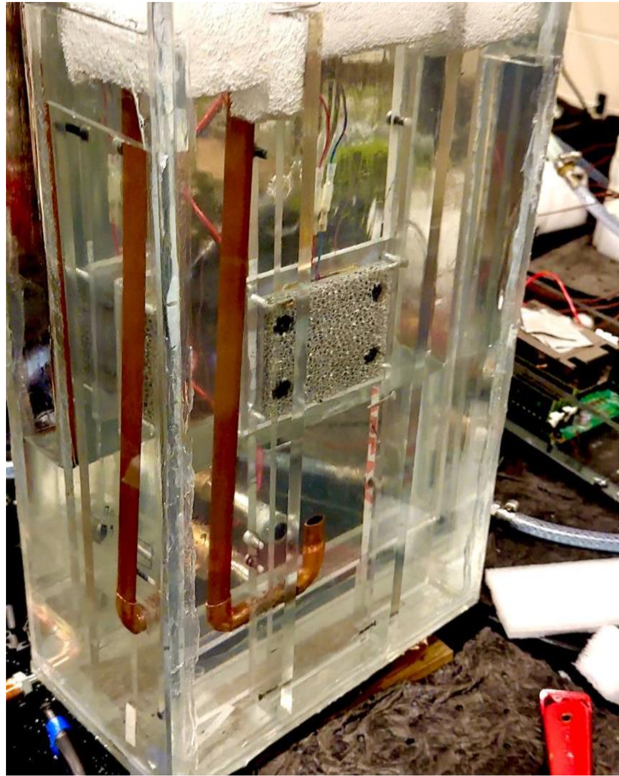

Figure:25. Thermal Test Chamber (EMNSPC UTA)

Methodology:

In this study, heat transfer experiments were conducted to assess the thermal-hydraulic efficiency of metal foam with PPI values of 5, 10, 20, and 40. The properties of the foam are detailed in the Foam tables below. The Flow rate, heat flux, and inlet temperature varied between 1 and 3 lpm, Heat flux: 19 W/cm^2 and 23.8 W/cm^2, respectively. In conjunction with the Data acquisition software, the Agilent 34972A data acquisition device was employed to facilitate real-time data reporting and continuous temperature monitoring. The program records the sample rate as well as temperatures, rate of flow, and pressure data every ten seconds for the course of the experiment, following the attainment of steady state. Following each experiment, the power source of the heater was deactivated, and the system was left to decrease in temperature until the outlet and inlet fluid temperatures were equivalent. Once the system achieves an equilibrium, the subsequent series of experiments commences with the heater being powered on, and the process of data collection is reiterated.

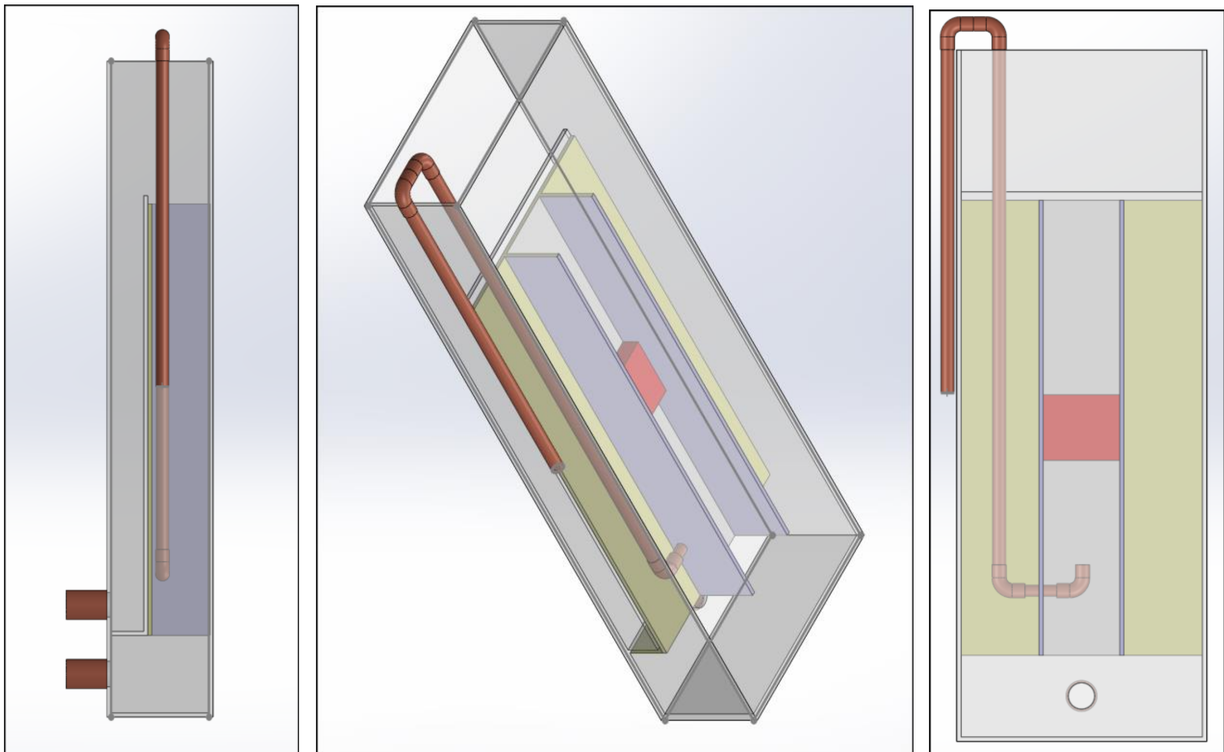

Figure: 26. Test setup **CAD** Design side view, isometric view and front view.

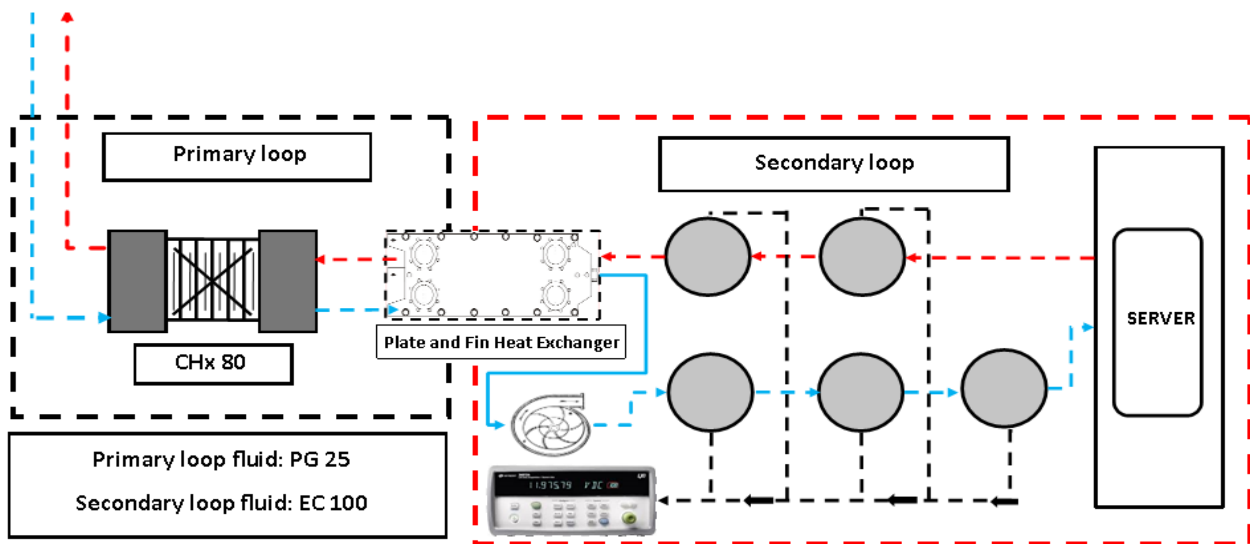

Figure: 27. Schematic Sketch of Thermal Test Vehicle.

Metal foam Properties:

Flow Span (W)	Flow Length (L)	Fin Height (H)	PPI	Starting Relative Density	Initial Relative Density (Actual)	Final Relative Density (Actual)	Cell Size	Pore Size	Ligament Thickness (d_f)
[in]	[in]	[in]	[-]	[%]	[%]	[%]	[mm]	[mm]	[mm]
3	3.5	0.75	5	10-12%	12.2%	12.2%	5.8	2.5	0.63
3	3.5	0.75	10	10-12%	12.3%	12.3%	4.4	1.9	0.55
3	3.5	0.75	20	10-12%	10.7%	10.7%	3.4	1.5	0.38
3	3.5	0.75	40	10-12%	11.2%	11.2%	2.2	1.1	0.31
3	3.5	0.5	5	10-12%	12.2%	12.2%	5.8	2.5	0.63
3	3.5	0.5	10	10-12%	12.3%	12.3%	4.4	1.9	0.55
3	3.5	0.5	20	10-12%	10.7%	10.7%	3.4	1.5	0.38
3	3.5	0.5	40	10-12%	11.2%	11.2%	2.2	1.1	0.31

Table. 5. Specifications of Aluminum foam Heat sink. (Provided by manufacturer)

Flow Span (W)	Flow Length (L)	Fin Height (H)	PPI	Fin/Foam Area per Unit Volume (a_f)		Alloy	Alloy Thermal Conductivity	k_L (flow direction)	k_W	k_H (heat flux direction)
[in]	[in]	[in]	[-]	[in^2/in^3]	[m^2/m^3]	[-]	[W/m-K]	[W/m-K]	[W/m-K]	[W/m-K]
3	3.5	0.75	5	14	561	AL 6101-T6	218	8.87	8.87	8.9
3	3.5	0.75	10	16	627	AL 6101-T6	218	8.94	8.94	8.9
3	3.5	0.75	20	21	818	AL 6101-T6	218	7.78	7.78	7.8
3	3.5	0.75	40	24	955	AL 6101-T6	218	8.14	8.14	8.1
3	3.5	0.5	5	14	561	AL 6101-T6	218	8.87	8.87	8.9
3	3.5	0.5	10	16	627	AL 6101-T6	218	8.94	8.94	8.9
3	3.5	0.5	20	21	818	AL 6101-T6	218	7.78	7.78	7.8
3	3.5	0.5	40	24	955	AL 6101-T6	218	8.14	8.14	8.1

Table. 6. Specifications of Aluminum foam Heat sink. (Provided by manufacturer)

Procedure:

- To test heat transfers to evaluate thermal performance of 5, 10, 20 and 40 PPI foam cores. The Agilent data acquisition system was used.
- Once the test system reaches stable, the software records one reading in every 10 seconds that includes Temperature of heater plate, inlet temperature of fluid, outlet temperature of fluid. The flow rate and pressure potential.
- After 100 readings for each foam core under different LPM, the heater power source is turned off, and the system is set to get back the inlet outlet and heater plate temperature as same and constant.
- The same procedure is repeated turning the flow rate and heater plater power for rest of foam core samples.

Sensor Calibration:

Digital Pressure Sensor

- The **GP-M010** pressure sensor and a reference pressure gauge were attached to the left and right sides of the Pneumatic Comparison Test Pump.
- The hand pump was used to increase the pressure within the test rig.
- The spinning knob on the test pump was closed to maintain the test pump pressurized.
- The pressure readings from the GP-M010 pressure sensor and the reference pressure gauge can be recorded.

Flow Sensor

- Introducing a known flow rate through the sensor using the reference standard. This flow rate should be within the operating range of the sensor.
- Recording the sensor's output at this known flow rate.

- Comparing the recorded sensor output to the actual flow rate and calculating the calibration error as the difference between the measured and actual flow rates.

Thermistor and thermocouple

- Temperature recorded for varying pool water temperature to calculate uncertainty.

CHAPTER 7

Result and Discussions

The experimental data pertains to the pressure difference across the heat sink, overall surface area efficiency, thermal resistance, and global heat transfer coefficient HTC*. In determining the heat transfer performance of the foams, the overall surface area effectiveness is a crucial characteristic. The temperature of metal foams decreases exponentially as one moves away from the heated base. In consequence, the metallic foams investigated exhibit significantly low surface heat transfer area efficiency. Equation 7 is utilized to calculate the overall surface efficiency in the present investigation; this value is contingent upon the fin parameter (m) and fin efficiency (n_f). It is evident that an increase in the number of pores per inch results in a decrease in overall surface area efficiency. Furthermore, efficiency decreases as the flow rate increases. Comparing all four foam samples reveals that the surface area efficiency of foams containing 5 PPI and 10 PPI is significantly greater than that of foams containing 20 PPI and 40 PPI. The heat sink's height is excessively high, as indicated by the overall surface area efficiency plot. Furthermore, the arithmetic means of HTC* indicates that any height from 0.5 to 0.75 will result in an identical value of HTC*.

The coefficient of convective heat transfer serves as an indicator of the porous heat sink's thermal effectiveness. The authors were able to examine the influence of foam structure on the emergence of thermal phenomena, which were quantified as global HTCs (air mass flow rate, pore size, and temperature). The effect of flow rate on the global and local heat transfer coefficients for different PPI heat sinks is illustrated in graphs. The heat fluxes utilized were 19 W/cm^2 and 23.8 W/cm^2respectively, at inlet temperature of 40°C. The variation in pore density among the four heat sinks is minimal.

While the HTC* value exhibits an increase in response to flow rate, it experiences a marginal decrease as the fluid inlet temperature rises. The data indicate that the HTC* increases with flow rate and is independent of the imposed heat flux. Results illustrate that the local heat transfer coefficients of 5 PPI and 10 PPI are nearly identical under all conditions when the flow rate is low. The 10 PPI heat sink outperformed the 40 PPI and 20 PPI heat sinks in every test, despite its smaller surface area. This could be attributed to the fact that 10 PPI foams facilitate effective thermal exchange by generating optimal turbulence conditions.

Based on the geometric information provided in the foam tables, it can be observed that the heat transfer area of the 40 PPI sample is five times larger than that of the 5 PPI metal foam. However, under all conditions, the global heat transfer coefficient (GHTC) of 5 PPI is greater than that of 40 PPI. This result was also calculated in a study conducted by Mancin et al. (2010) and is calculated as the product of the total heat transfer area, the local heat transfer coefficient, and the overall surface efficiency of 5 PPI. Approximately 2% is the maximum percentage difference between the values of HTC* for all boundary conditions. For inlet temperatures of 40 °C, the corresponding patterns are observed at 19 W/cm^2 and 23.8 W/cm^2.

Utilizing Equation 3, the resistance to heat of the foams is computed. It is evident that 10 PPI foams exhibit the lowest thermal resistance under all flow conditions, while 40 PPI foams demonstrate the highest thermal resistance. Furthermore, as flow rate increases, the thermal resistance also diminishes. The relationship between thermal resistance and the heat transfer coefficient is inversely correlated, so the thermal resistance value corresponds to the values shown in graphs.

As both the flowing rate and PPI increase, pressure drops also increase. It is possible to derive three crucial parameters—the permeability K, the form coefficient C, and the inertia coefficient f—from the pressure drop. At extremely low velocities, characterized by Darcy flow, a pressure gradient is proportional to the velocity (permeability K). However, at high velocities, separation from Darcy flow is caused by turbulence and form drag and is proportional to the inertia coefficient. Furthermore, as the cell diameter or PPI increases, there is a corresponding increase in the form coefficient (C) and a decrease in permeability (K), both of which are inversely related to the pressure drop differential (Beavers and Sparrow, 1969).

The experimental manifestation of this phenomenon is discernible through the measurement of pressure drop; among all the foams, 5 PPI demonstrates the most favorable performance due to its lowest pressure drop. This aligns with the author's logical explanations regarding the physical significance of the permeation and momentum coefficients. 1.5 to 1.8 times the greater pressure drop occurs across 40 PPI foam compared to 5 PPI foam, encompassing all heat fluxes and inlet fluid temperatures. The anticipated behavior described can be ascribed to the metal foam's pore size and distribution.

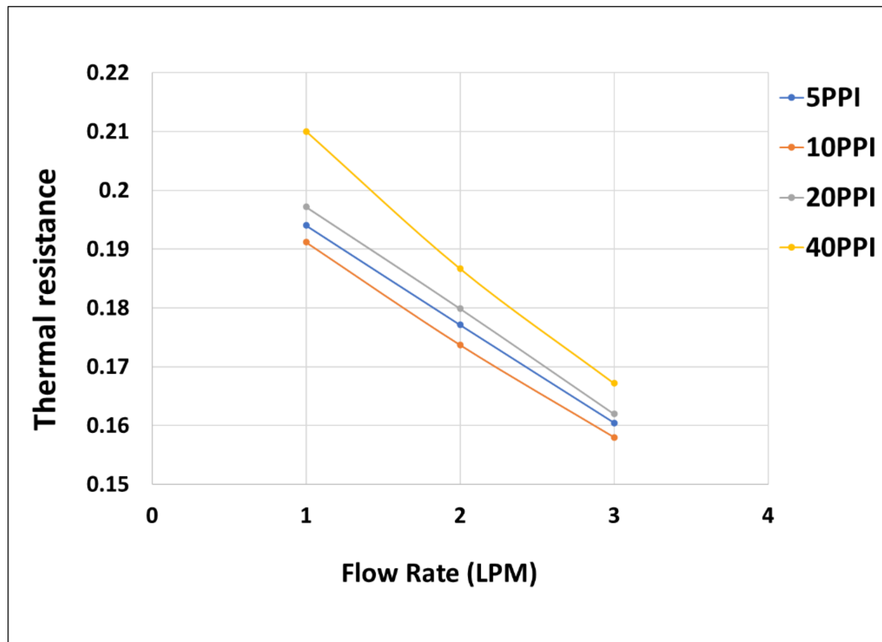

Graph:1. Thermal Resistance vs Flow Rate for Inlet Fluid temperature, Power, and Foam core height as 40°*C*, 200 Watts and 0.5 inch respectively.

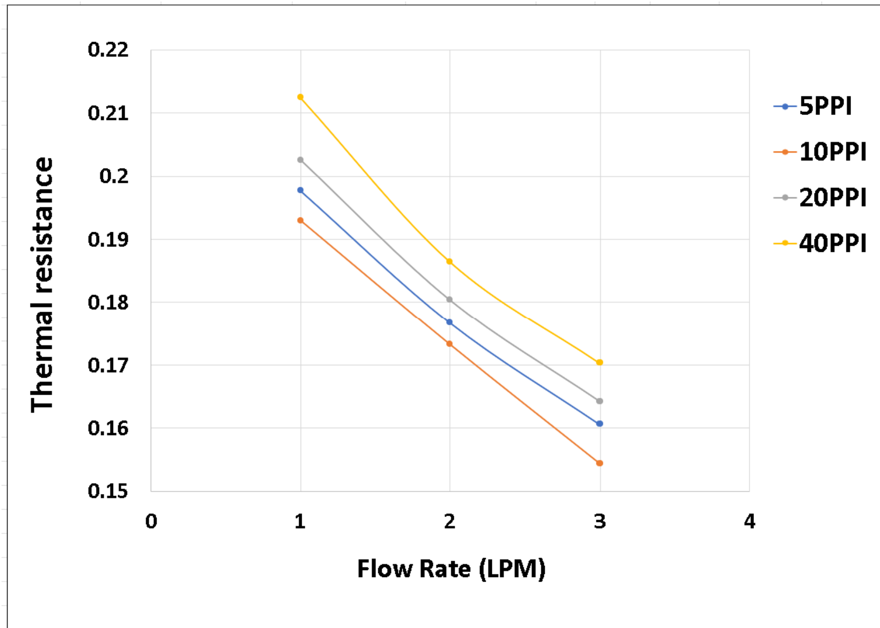

Graph:2. Thermal Resistance vs Flow Rate for Inlet Fluid temperature, Power, and Foam core height as 40°C, 250 Watts and 0.5 inch respectively.

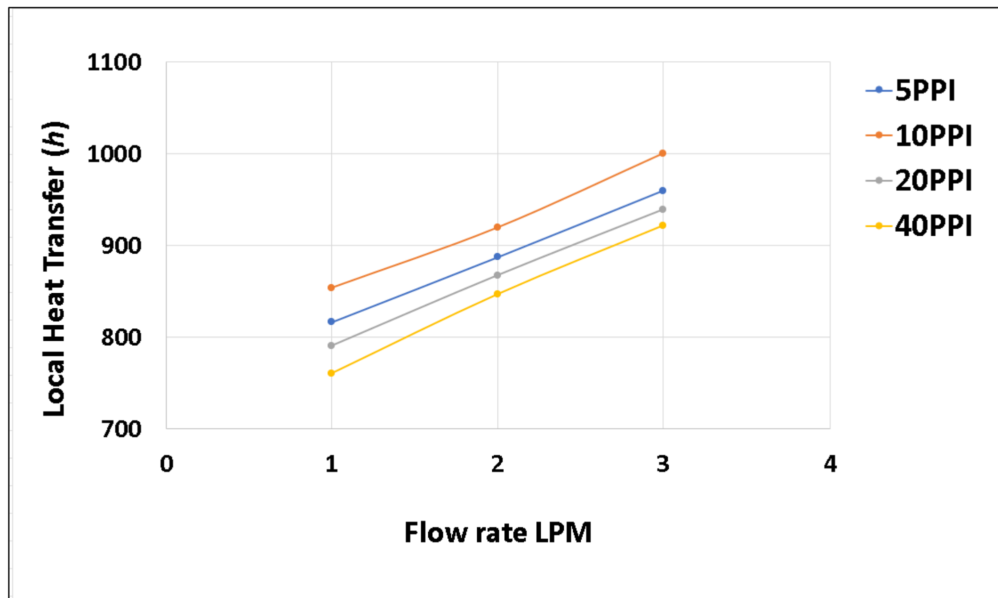

Graph:3. Local Heat Transfer vs Flow Rate for Inlet Fluid temperature, Power, and Foam core height as 40°C, 200 Watts and 0.5 inch respectively.

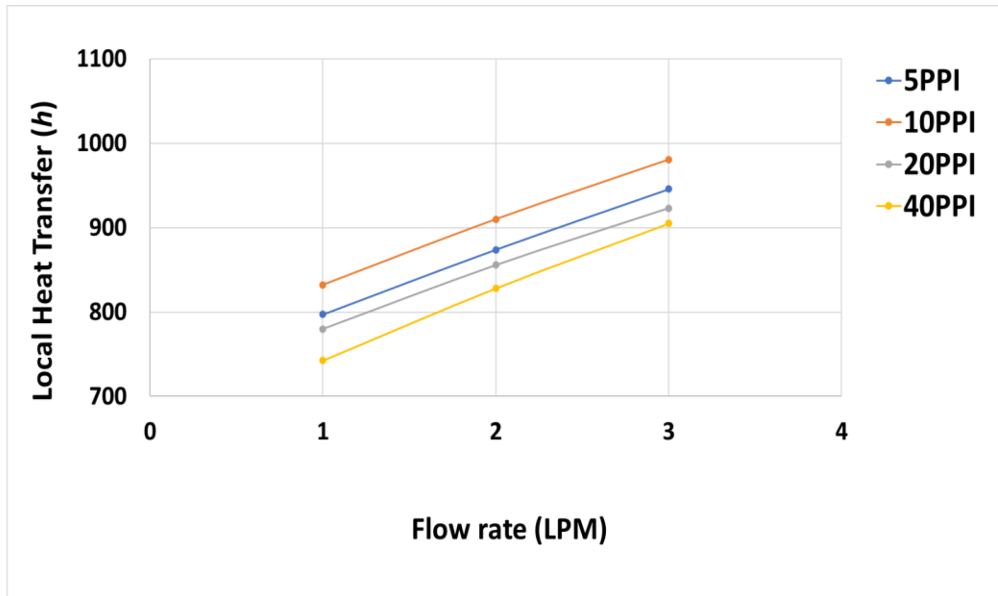

Graph:4. Local Heat Transfer vs Flow Rate for Inlet Fluid temperature, Power, and Foam core height as 40°C, 250 Watts and 0.5 inch respectively.

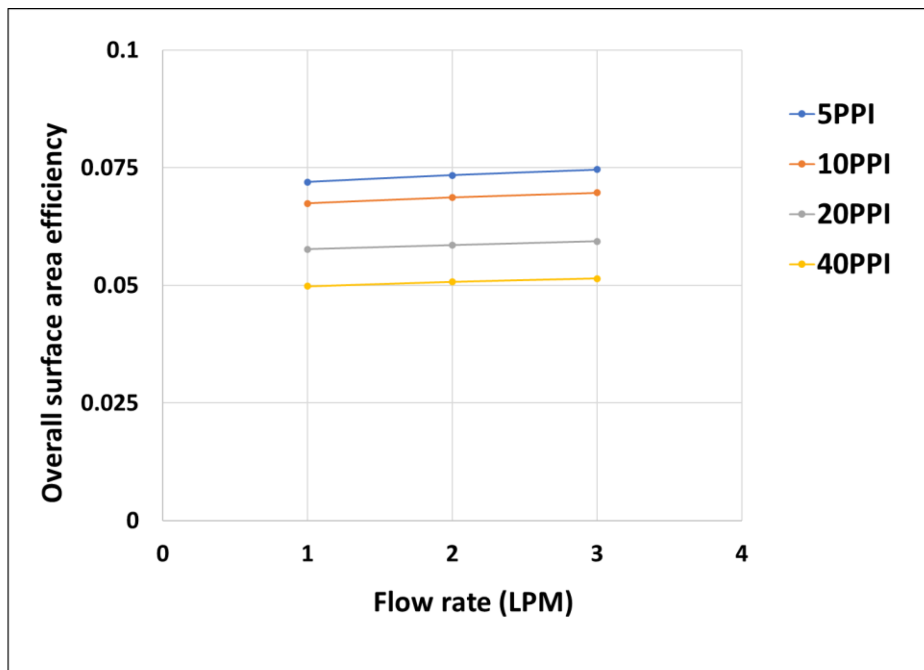

Graph:5. Overall surface area efficiency vs Flow Rate for Inlet Fluid temperature, Power, and Foam core height as 40°C, 200 Watts and 0.5 inch respectively.

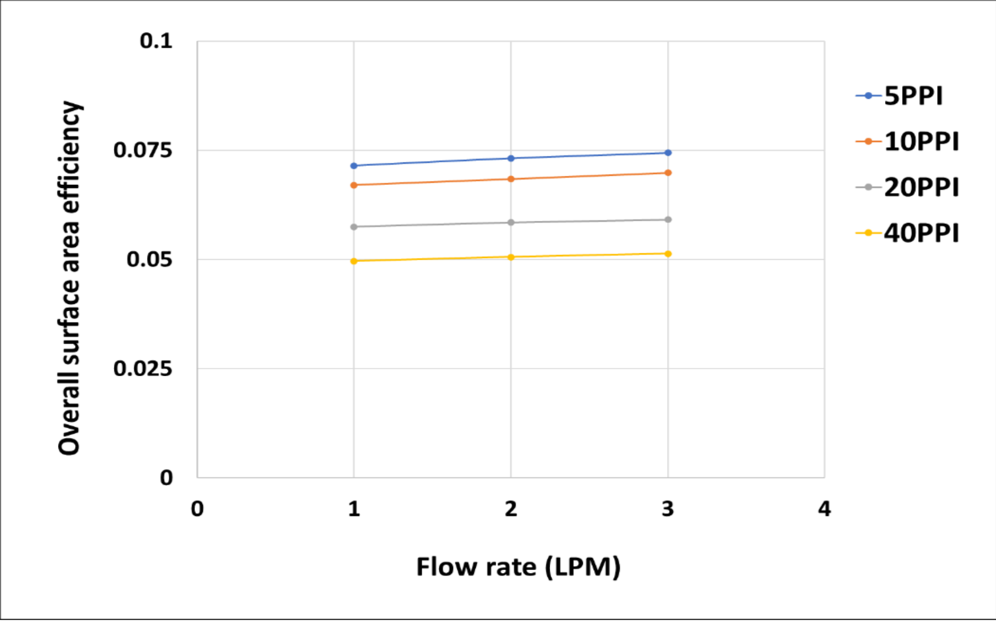

Graph:6. Overall surface area efficiency vs Flow Rate for Inlet Fluid temperature, Power, and Foam core height as 40°C, 250 Watts and 0.5 inch respectively.

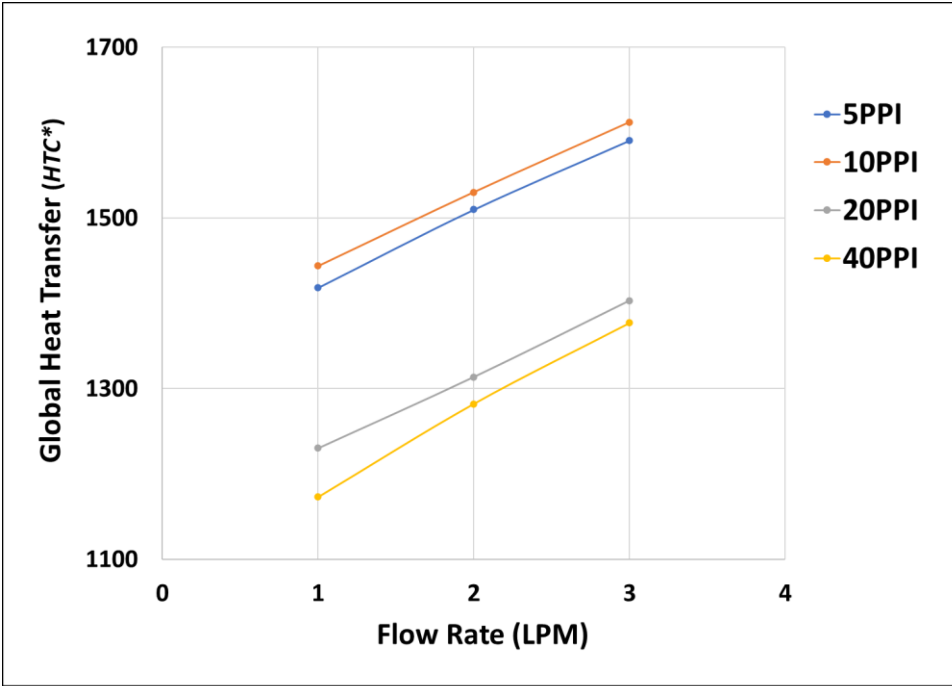

Graph:7. Global Heat Transfer coefficient vs Flow Rate for Inlet Fluid temperature, Power, and Foam core height as 40°C, 200 Watts and 0.5 inch respectively.

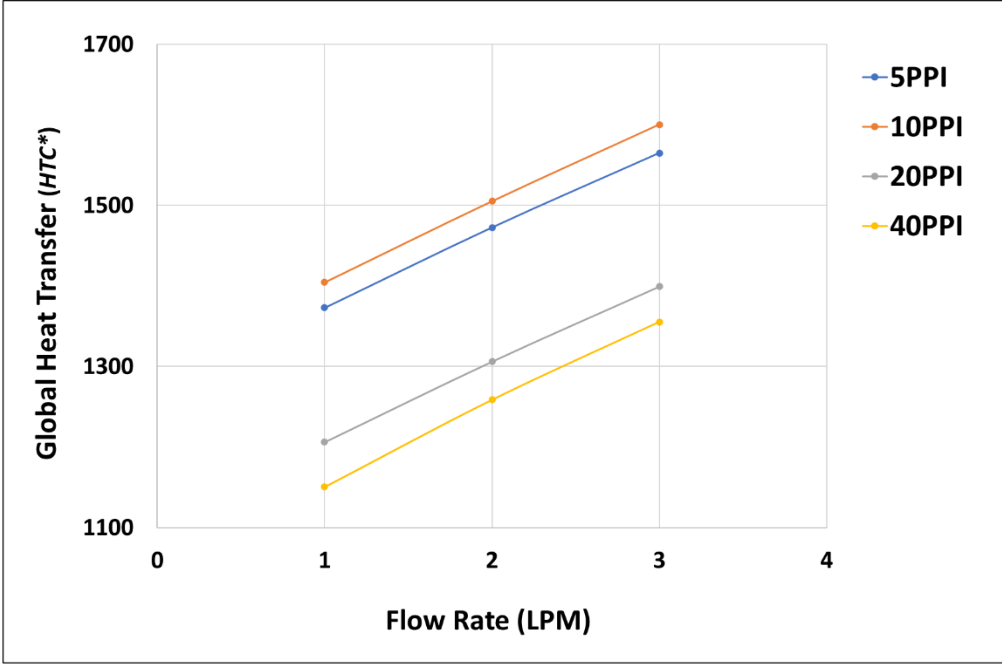

Graph:8. Global Heat Transfer coefficient vs Flow Rate for Inlet Fluid temperature, Power, and Foam core height as 40°C, 250 Watts and 0.5 inch respectively.

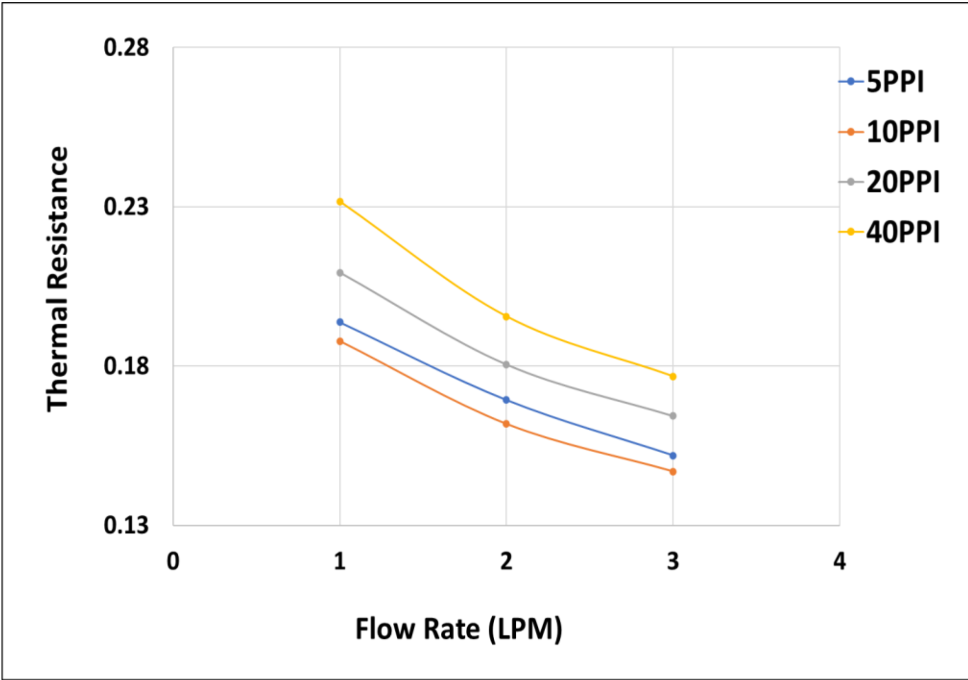

Graph:9. Thermal Resistance vs Flow Rate for Inlet Fluid temperature, Power, and Foam core height as 40°C, 200 Watts and 0.75 inch respectively.

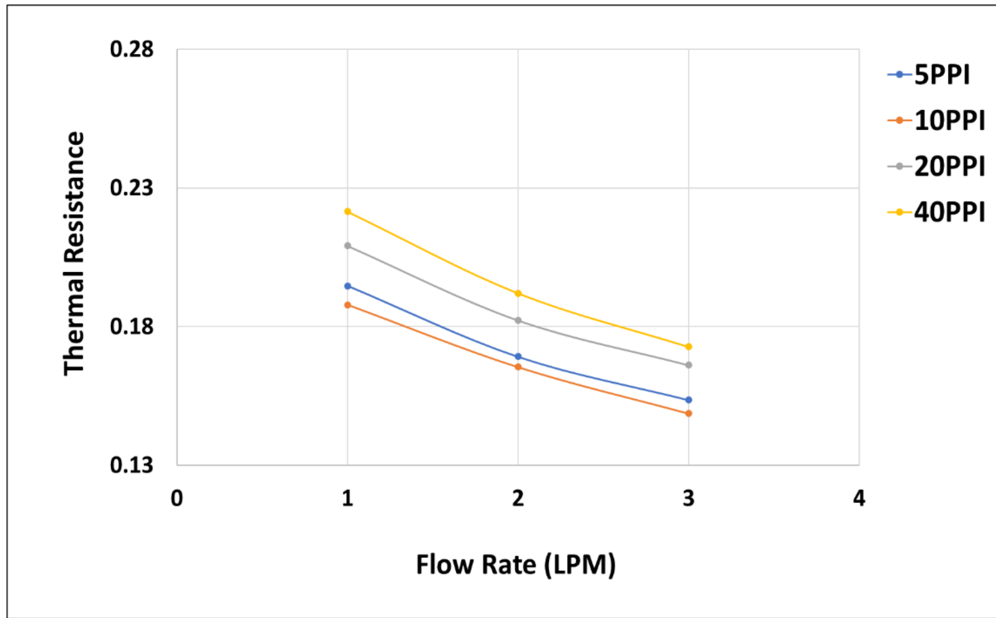

Graph:10. Thermal Resistance vs Flow Rate for Inlet Fluid temperature, Power, and Foam core height as 40°C, 250 Watts and 0.75 inch respectively.

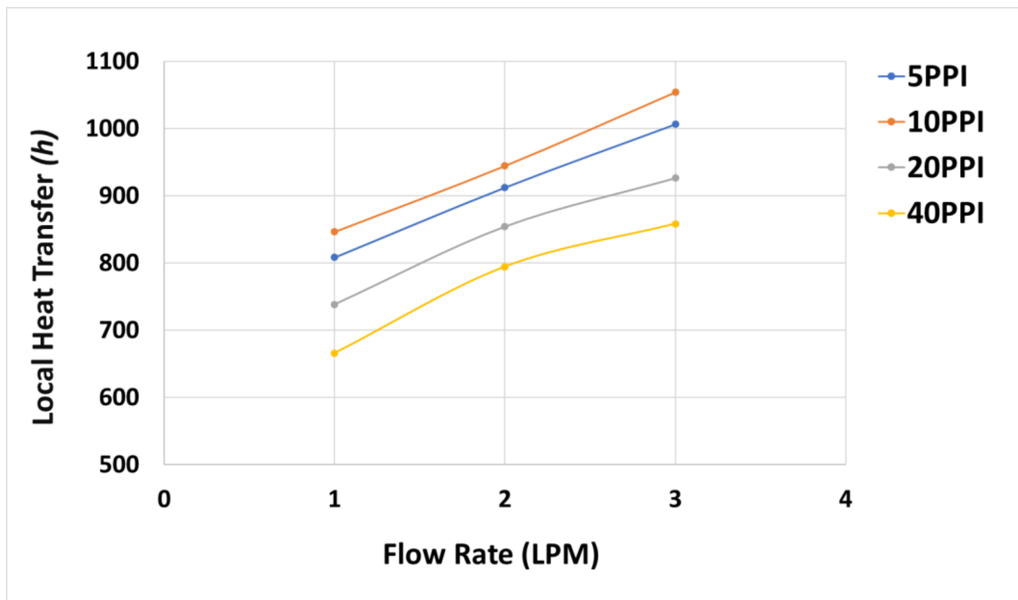

Graph:11. Local Heat Transfer (h) vs Flow Rate for Inlet Fluid temperature, Power, and Foam core height as 40°C, 200 Watts and 0.75 inch respectively.

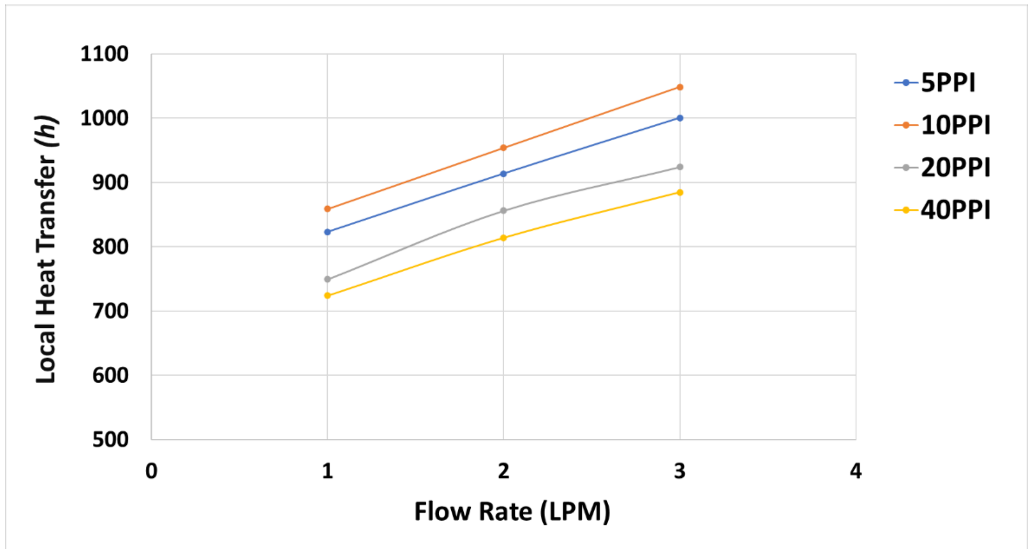

Graph:12. Local Heat Transfer (h) vs Flow Rate for Inlet Fluid temperature, Power, and Foam core height as 40°C, 250 Watts and 0.75 inch respectively.

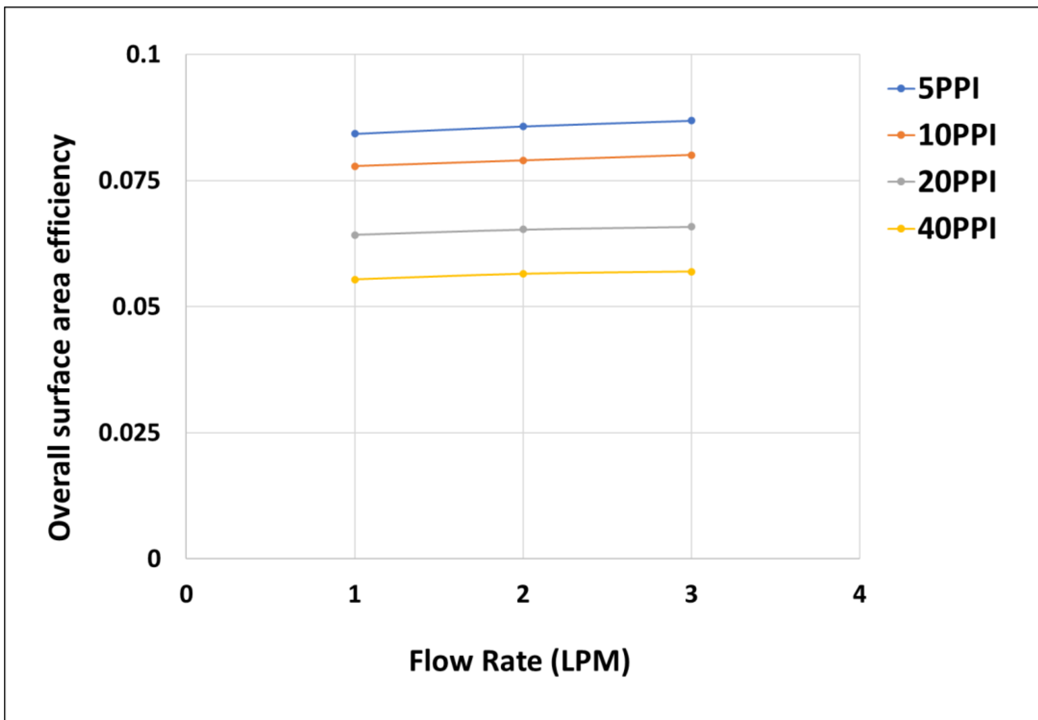

Graph:13. Overall Surface Area Efficiency vs Flow Rate for Inlet Fluid temperature, Power, and Foam core height as 40°C, 200 Watts and 0.75 inch respectively.

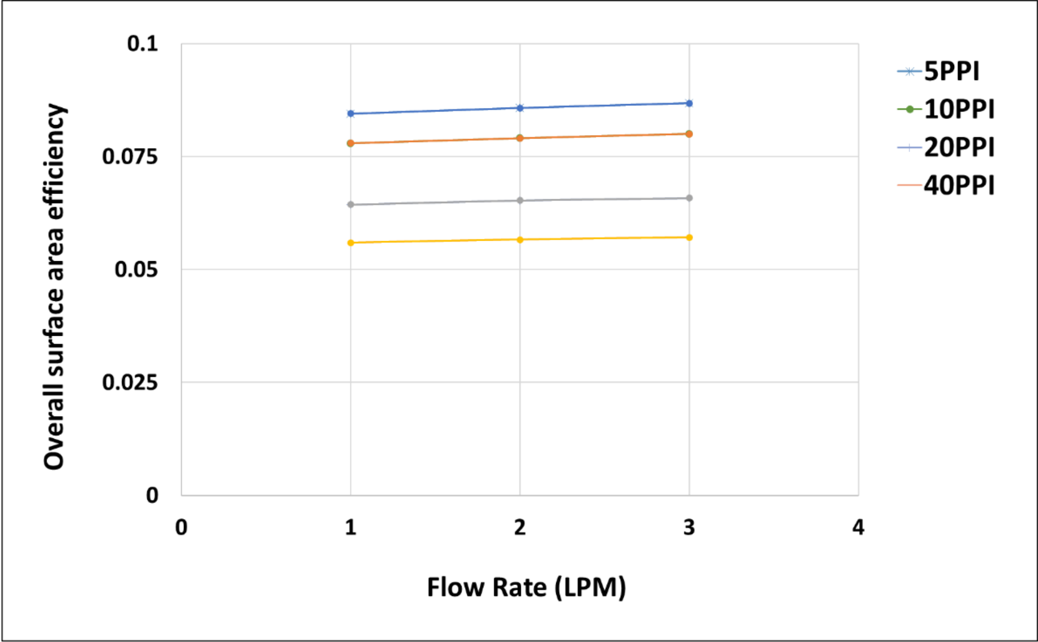

Graph:14. Overall Surface Area Efficiency vs Flow Rate for Inlet Fluid temperature, Power, and Foam core height as 40°C, 250 Watts and 0.75 inch respectively.

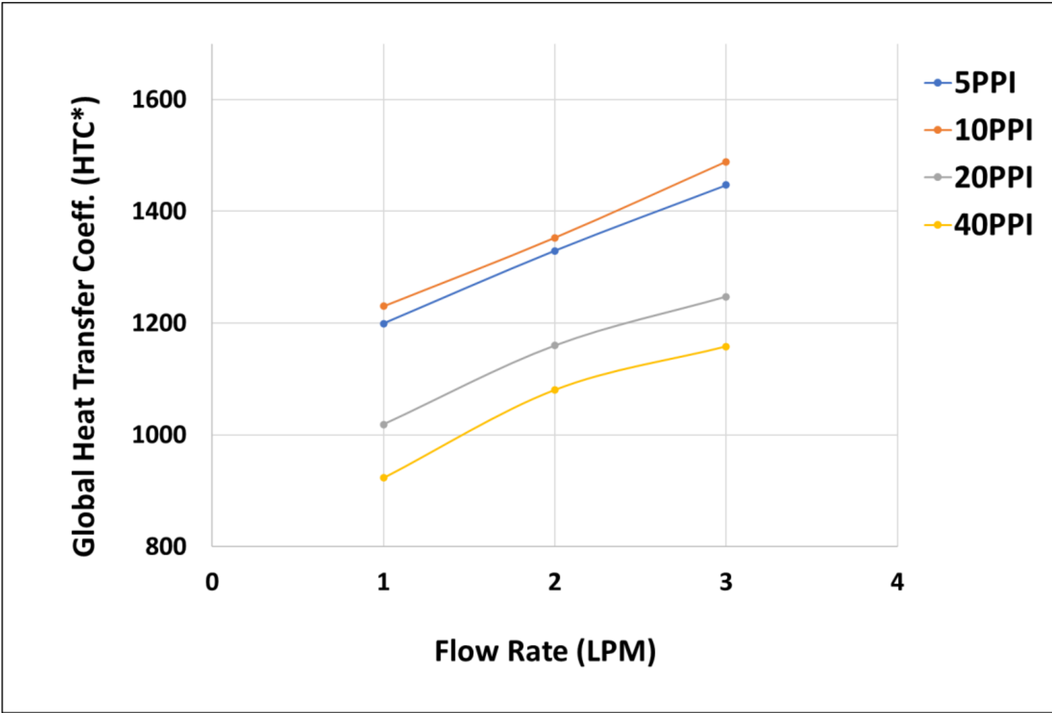

Graph:15. Global Heat Transfer vs Flow Rate for Inlet Fluid temperature, Power, and Foam core height as 40°C, 200 Watts and 0.75 inch respectively.

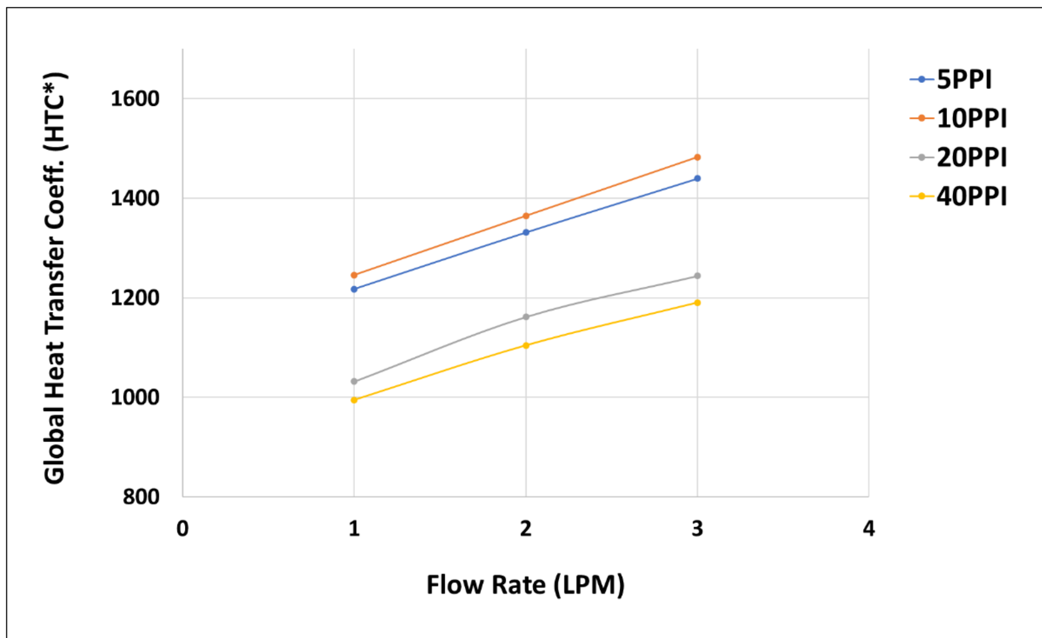

Graph:16. Global Heat Transfer vs Flow Rate for Inlet Fluid temperature, Power, and Foam core height as 40°C, 250 Watts and 0.75 inch respectively.

CHAPTER 8

Conclusions

The findings of this study pertain to the heat transfer and pressure drop characteristics of aluminum metal foam with cores measuring 0.5 and 0.75 inches in height and porosities of 5, 10, 20, and 40 PPI (pores per inch), while maintaining an almost constant porosity. The experimental findings are documented with respect to pressure drop, overall surface area efficiency, global heat transfer coefficient, and thermal resistance. The experimental findings were obtained for two distinct heat fluxes 19 W/cm^2 and 23.8 W/cm^2, through the manipulation of the fluid flow rate and inlet fluid temperature (ranging from 1 LPM to 3 LPM) and 40°C, respectively.

As the mass flow rate increases, the global transfer of heat coefficient does not fluctuate in response to changes in heat flux.

Thermal Resistance: The 10PPI has lowest thermal resistance and has highest global and local heat transfer coefficient, while 40PPI Foam has highest thermal resistance and exhibited lowest in both local and global heat transfer coefficient.

Overall surface area efficiency: 5PPI exhibited lowest overall surface area efficiency.

Heat transfer coefficient: The local heat transfer (h) is lower than global heat transfer (HTC*)

Height: When comparing the core height, 0,75 inch has lower thermal resistance as compared to 0.5-inch height core. While in terms of overall surface area efficiency 0.75 inch has a higher value.

Flow rate: Increasing the Flow rate increases the heat transfer coefficient while decreasing thermal resistance under the boundary conditions.

Pressure Drop: 5PPI and 40 PPI foam has lowest, and highest pressure drop ΔP respectively.

The potential thermal management application necessitates an optimization procedure, which demands an in-depth comprehension of their heat transfer characteristics. Additionally, it is necessary to develop an analytical model that can forecast the coefficient of heat transfer and pressure drop in order to completely describe and optimize the heat sink design of metal foams.

BIOGRAPHICAL STATEMENT

"Beforehanding his academic career, Manish Kumawat, emerged in the field of engineering, obtained a bachelor's degree in mechanical engineering from Rajasthan Technical University. His enthusiasm for engineering was additionally stimulated by practical experience acquired during product engineering role at reputable organization, where he refined his abilities and implemented his knowledge in the real-world. Manish distinguished himself professionally in the fall of 2021 by commencing a master's program in Aerospace Engineering at the esteemed University of Texas at Arlington. This choice not only broadened his scholarly perspectives but also granted him the opportunity to engage in research projects. In his capacity as a volunteer research assistant at the Electronics MEMS and Nanoelectronics Systems Packaging Centre, Manish undertook a captivating investigation into the cooling effects of metal-foam immersed in fluid. His investigation extended beyond a mere scientific endeavor; that included an investigation of the metal foam's reliability and performance under coolant flow. Manish's research, which was conducted with great attention under support of his professor and mentor led him detailed in regard of the performance, dependability, and effective in thermal management, he established him as a highly prospective scholar in the discipline. Anticipating the culmination of his master's program, he is enthusiastic about advancing his vocation in thermal heating and cooling solutions with the goal of providing the industry with sustainable solutions and novel concepts.

REFERENCES:

[1]. Bar-Cohen, A., & Wang, P. (2012). Thermal management of on-chip hot spot. *Journal of Heat Transfer*, 134(5). https://doi.org/10.1115/1.4005708

[2]. Mancin, S., Zilio, C., Diani, A., & Rossetto, L. (2013). Air forced convection through metal foams: Experimental results and modeling. *International Journal of Heat and Mass Transfer*, 62, 112–123. https://doi.org/10.1016/j.ijheatmasstransfer.2013.02.050

[3]. Boyd, B. and Hooman, K., 2012. Air-cooled micro-porous heat exchangers for thermal management of fuel cells. *International Communications in Heat and Mass Transfer*, *39*(3), pp.363-367.

[4]. Habibi Khalaj, Ali, and Saman K. Halgamuge. "A review on efficient thermal management of air- and liquid-cooled data centers: From chip to the cooling system." *Applied Energy*, vol. 205, 2017, pp. 1165–1188, https://doi.org/10.1016/j.apenergy.2017.08.037.

[5]. Singh, R., Akbarzadeh, A. and Mochizuki, M. (2009) "Sintered porous heat sink for cooling of high-powered microprocessors for server applications," *International journal of heat and mass transfer*, 52(9–10), pp. 2289–2299. doi: 10.1016/j.ijheatmasstransfer.2008.11.016.

[6]. Lee, Y.J., Singh, P.K. and Lee, P.S., 2015. Fluid flow and heat transfer investigations on enhanced microchannel heat sink using oblique fins with parametric study. *International Journal of Heat and Mass Transfer*, 81, pp.325-336.

[7]. Dede, E.M. and Liu, Y., 2013. Experimental and numerical investigation of a multi-pass branching microchannel heat sink. *Applied Thermal Engineering*, 55(1-2), pp.51-60.

[8]. Zhang, Zhihao, et al. "A review of the state-of-the-art in Electronic Cooling." *E-Prime - Advances in Electrical Engineering, Electronics and Energy*, vol. 1, 2021, p. 100009, https://doi.org/10.1016/j.prime.2021.100009.

[9]. Murshed, S.S. and De Castro, C.N., 2017. A critical review of traditional and emerging techniques and fluids for electronics cooling. *Renewable and Sustainable Energy Reviews*, 78, pp.821-833.

[10]. Meng, X., Zhu, J., Wei, X. and Yan, Y., 2018. Natural convection heat transfer of a straight-fin heat sink. *International Journal of Heat and Mass Transfer*, *123*, pp.561-568.

[11]. Scott, A.W., 1974. Cooling of electronic equipment. *(No Title)*.

[12]. El Alami, M., Najam, M., Semma, E., Oubarra, A. and Penot, F., 2005. Electronic components cooling by natural convection in horizontal channel with slots. *Energy conversion and Management,* 46(17), pp.2762-2772.

[13]. Cengel, A., 2003. Heat transfer. New York: McGraw-Hill.

[14]. Liang, G. and Mudawar, I., 2017. Review of spray cooling–Part 1: Single-phase and nucleate boiling regimes, and critical heat flux. *International Journal of Heat and Mass Transfer*, 115, pp.1174-1205.

[15]. Cader, T., Westra, L.J. and Eden, R.C., 2004. Spray cooling thermal management for increased device reliability. *IEEE Transactions on Device and Materials Reliability*, 4(4), pp.605-613.

[16]. Gangoli Rao, Arvind & Yeshayahou, Levy & Kitron-Belinkov, Myra. (2009). Heat transfer characteristics of a multiple jet impingement system. 1. 314-328.

[17]. Tepe, A.Ü., Yetişken, Y., Uysal, Ü. and Arslan, K., 2020. Experimental and numerical investigation of jet impingement cooling using extended jet holes. International Journal of Heat and Mass Transfer, 158, p.119945.

[18]. Sabato, M., Fregni, A., Stalio, E., Brusiani, F., Tranchero, M. and Baritaud, T., 2019. Numerical study of submerged impinging jets for power electronics cooling. *International Journal of Heat and Mass Transfer*, 141, pp.707-718.
[19]. Wu, R., Hong, T., Cheng, Q., Zou, H., Fan, Y. and Luo, X., 2019. Thermal modeling and comparative analysis of jet impingement liquid cooling for high power electronics. *International Journal of Heat and Mass Transfer*, 137, pp.42-51.
[20]. Nadda, R., Kumar, A. and Maithani, R., 2018. Efficiency improvement of solar photovoltaic/solar air collectors by using impingement jets: A review. *Renewable and Sustainable Energy Reviews*, 93, pp.331-353.
[21]. Kuncoro, I.W., Pambudi, N.A., Biddinika, M.K., Widiastuti, I., Hijriawan, M. and Wibowo, K.M., 2019, December. Immersion cooling as the next technology for data center cooling: A review. *In Journal of Physics: Conference Series* (Vol. 1402, No. 4, p. 044057). IOP Publishing.
[22]. Wei, J., 2019, November. Liquid Cooling, opportunity & challenges toward effective and efficient scalabilities. In 2019 IEEE CPMT Symposium Japan (ICSJ) (pp. 83-84). IEEE.
[23]. Wang, J.X., Li, Y.Z., Li, J.X., Li, C., Xiong, K. and Ning, X.W., 2018. Enhanced heat transfer by an original immersed spray cooling system integrated with an ejector. Energy, 158, pp.512-523.
[24]. Patil, M.S., Seo, J.H. and Lee, M.Y., 2021. A novel dielectric fluid immersion cooling technology for Li-ion battery thermal management. *Energy Conversion and Management,* 229, p.113715.
[25]. Qu, W. and Mudawar, I., 2003. Measurement and prediction of pressure drop in two-phase micro-channel heat sinks. *International Journal of Heat and Mass Transfer*, 46(15), pp.2737-2753.
[26]. Kandlikar, S.G. and Upadhye, H.R., 2005, March. Extending the heat flux limit with enhanced microchannels in direct single-phase cooling of computer chips. *In Semiconductor Thermal Measurement and Management IEEE Twenty First Annual IEEE Symposium*, 2005. (pp. 8-15). IEEE.
[27]. Marto, P.J. and Lepere, V.J., 1982. Pool boiling heat transfers from enhanced surfaces to dielectric fluids.
[28]. Cheng, C.C., Chang, P.C., Li, H.C. and Hsu, F.I., 2020. Design of a single-phase immersion cooling system through experimental and numerical analysis. *International Journal of Heat and Mass Transfer,* 160, p.120203.
[29]. Li, J., 2020. Current commercialization status of electrowetting-on-dielectric (EWOD) digital microfluidics. Lab on a Chip, 20(10), pp.1705-1712.
[30]. Chen, L. and Bonaccurso, E., 2014. Electrowetting—From statics to dynamics. Advances in colloid and interface science, 210, pp.2-12.
[31]. Nelson, W.C., and Kim, C.J.C., 2012. Droplet actuation by electrowetting-on-dielectric (EWOD): A review. Journal of Adhesion Science and Technology, 26(12-17), pp.1747-1771.
[32]. Silverio, Vania. (2015). Microchannel Cooling Technologies. 10.13140/RG.2.1.2960.0721.
[33]. Mehendale, S.S., Jacobi, A.M., and Shah, R.K., 2000. Fluid flow and heat transfer at micro-and meso-scales with application to heat exchanger design.
[34]. Kandlikar, S.G. and Grande, W.J., 2003. Evolution of microchannel flow passages--thermohydraulic performance and fabrication technology. Heat transfer engineering, 24(1), pp.3-17.

[35]. van Erp, Remco et al. “Efficient Microchannel Cooling of Multiple Power Devices with Compact Flow Distribution for High Power-Density Converters.” IEEE Transactions on Power Electronics 35 (2020): 7235-7245.
[36]. Garner, S.D., 1996. Heat pipes for electronics cooling applications. Electronics Cooling, 2, pp.18-23.
[37]. Chen, X., Ye, H., Fan, X., Ren, T. and Zhang, G., 2016. A review of small heat pipes for electronics. Applied Thermal Engineering, 96, pp.1-17.
[38]. Simons, R.E. and Chu, R.C., 2000, March. Application of thermoelectric cooling to electronic equipment: a review and analysis. In the Sixteenth Annual IEEE Semiconductor Thermal Measurement and Management Symposium (Cat. No. 00CH37068) (pp. 1-9). IEEE.
[39]. Zebarjadi, M., 2015. Electronic cooling using thermoelectric devices. Applied Physics Letters, 106(20).
[40]. Sangchandr, B. and Afzulpurkar, V., 2009. A novel approach for cooling electronics using a combined heat pipe and thermoelectric module. J. Eng. Appl. Sci, 2(4), pp.603-610.
[41]. Li, W., Li, L., Cui, W., & Guo, M. Experimental investigation on the thermal performance of vapor chamber in a compound liquid cooling system. International Journal of Heat and Mass Transfer, 170. https://doi.org/10.1016/j.ijheatmasstransfer.2021.121026
[42]. Velardo, Jason & Singh, Randeep & Date, Ashwin & Date, Abhijit. (2017). An Investigation into the Effective Thermal Conductivity of Vapor Chamber Heat Spreaders. Energy Procedia. 110. 256-261. 10.1016/j.egypro.2017.03.136.
[43]. Fleischer, A.S., 2015. Thermal energy storage using phase change materials: fundamentals and applications. Springer.
[44]. Pal, A., Joshi, Y.K., Beitelmal, M.H., Patel, C.D., and Wenger, T.M., 2002. Design and performance evaluation of a compact thermosyphon. IEEE Transactions on Components and Packaging Technologies, 25(4), pp.601-607.
[45]. Jaworski, M. and Domañski, R., 2006, May. A novel design of heat sink with PCM for electronics cooling. In 10th International Conference on Thermal Energy Storage, Stockton (Vol. 31).
[46]. Mohapatra, S.C. and Loikits, D., 2005, March. Advances in liquid coolant technologies for electronics cooling. In Semiconductor Thermal Measurement and Management IEEE Twenty First Annual IEEE Symposium, 2005. (pp. 354-360). IEEE.
[47]. Mohapatra, S.C., 2006. An overview of liquid coolants for electronics cooling. Electronics cooling, 12(2), p.22.
[48]. https://info.engineeredfluids.com/hubfs/%20Documentation/Safety%20Data%20Sheets ElectroCool%20SDS/ElectroCool%20EC100%20-%20(EC-100-SDS-ENG-GHS 20230512).pdf?utm_referrer=https%3A%2F%2Fwww.engineeredfluids.com%2F
[49]. Banhart, J 2001, ‘Manufacture, characterization and application of cellular metals and metal foams’, Progress in Materials Science, vol. 46, pp. 559–632.
[50]. Ramay, HR & Zhang, M 2003, ‘Preparation of porous hydroxyapatite scaffolds by combination of the gel-casting and polymer sponge methods’, Journal of Biomaterials, vol. 24, no. 10, pp. 3293–3302
[51]. Tulasiram, N, Kumar, KS & Kumar, A 2017, ‘A review on the manufacturing processes of aluminum metal foams and its applications’, International Journal of Current Engineering and Scientific Research (IJCESR), vol. 4, no. 12, pp. 1–4.
[52]. Yuan, W, Tang, Y, Yang, X & Wan, Z 2012, ‘Porous metal materials for polymer electrolyte membrane fuel cells- A review’, Applied Energy, vol. 94, pp. 309–329.

[53]. Mahajan, SM, & Ganesh AJ 2015, 'Aluminum Foaming for Lighter Structure', Int. J. Comput. Eng. Res, vol. 5, no. 1, pp. 70–74.
[54]. Banhart, J 2000, 'Metallic foams: challenges and opportunities, Fraunhofer-Institute for Advanced Materials, Bremen, Germany.
[55]. Akiyama, S, Ueno, H, Imagawa, K, Kitahara, A, Nagata, S, Morimoto, K, Nishikawa, T, Itoh, M & Amagasaki 1987, 'Foamed metal and method on producing same', US Patent No 4,713,277.
[56]. Miyoshi, T, Itoh, M, Akiyama, S & Kitahara, A 2000, 'ALPORAS aluminium foam: Production process, properties and application', Advanced Engineering Materials, vol. 2, no. 4, pp. 179–183.
[57]. Lee, CC 2005, 'Pembangunan dan penghasilan titanium berbusa', MSc thesis, Universiti Kebangsaan Malaysia, Bangi, Selangor
[58]. Gupta, G., Nair, V., Bansode, P., Suthar, R., Pundla, S.A., Herring, J., Lamotte-Dawaghreh, J., Sivaraju, K.B., Agonafer, D., Mynampati, P. and Sweeney, M., 2023, October. A Numerical Study Comparing Forced and Natural Convection in a High-Density Single-Phase Immersed Cooled Server. In *International Electronic Packaging Technical Conference and Exhibition* (Vol. 87516, p. V001T01A014). American Society of Mechanical Engineers.
[59]. Gupta, G., Nair, V., Pundla, S.A., Bansode, P., Suthar, R., Herring, J., Lamotte-Dawaghreh, J., Sivaraju, K.B., Agonafer, D., Mynampati, P. and Sweeney, M., 2023, October. Optimization of a Air-Cooled Heatsink for Immersion Cooling Application. In International Electronic Packaging Technical Conference and Exhibition (Vol. 87516, p. V001T01A013). American Society of Mechanical Engineers.